RESEARCH ARTICLE

Population clustering of structural brain aging and its association with brain development

Haojing Duan[1,2], Runye Shi[3], Jujiao Kang[1,2], Tobias Banaschewski[4], Arun LW Bokde[5], Christian Büchel[6], Sylvane Desrivières[7], Herta Flor[8,9], Antoine Grigis[10], Hugh Garavan[11], Penny A Gowland[12], Andreas Heinz[13], Rüdiger Brühl[14], Jean-Luc Martinot[15], Marie-Laure Paillère Martinot[15,16], Eric Artiges[15,17], Frauke Nees[4,8,18], Dimitri Papadopoulos Orfanos[10], Luise Poustka[19], Sarah Hohmann[4], Nathalie Nathalie Holz[4], Juliane Fröhner[20], Michael N Smolka[20], Nilakshi Vaidya[21], Henrik Walter[13], Robert Whelan[22], Gunter Schumann[1,21,23,24], Xiaolei Lin[3,25]*, Jianfeng Feng[1,2,3,23,26,27,28]*

[1]Institute of Science and Technology for Brain-Inspired Intelligence, Fudan University, Shanghai, China; [2]Key Laboratory of Computational Neuroscience and Brain-Inspired Intelligence (Fudan University), Ministry of Education, Shanghai, China; [3]School of Data Science, Fudan University, Shanghai, China; [4]Department of Child and Adolescent Psychiatry and Psychotherapy, Central Institute of Mental Health, Medical Faculty Mannheim, Heidelberg University, Mannheim, Germany; [5]Discipline of Psychiatry, School of Medicine and Trinity College Institute of Neuroscience, Trinity College Dublin, Dublin, Ireland; [6]University Medical Centre Hamburg-Eppendorf, Hamburg, Germany; [7]Social Genetic and Developmental Psychiatry Centre, Institute of Psychiatry, Psychology and Neuroscience, King's College London, London, United Kingdom; [8]Institute of Cognitive and Clinical Neuroscience, Central Institute of Mental Health, Medical Faculty Mannheim, Heidelberg University, Mannheim, Germany; [9]Department of Psychology, School of Social Sciences, University of Mannheim, Mannheim, Germany; [10]NeuroSpin, CEA, Université Paris-Saclay, Gif-sur-Yvette, France; [11]Departments of Psychiatry and Psychology, University of Vermont, Burlington, United States; [12]Sir Peter Mansfield Imaging Centre School of Physics and Astronomy, University of Nottingham, Nottingham, United Kingdom; [13]Department of Psychiatry and Psychotherapy CCM, Charité – Universitätsmedizin Berlin, corporate member of Freie Universität Berlin, Humboldt-Universität zu Berlin, and Berlin Institute of Health, Berlin, Germany; [14]Physikalisch-Technische Bundesanstalt (PTB), Braunschweig and Berlin, Berlin, Germany; [15]Institut National de la Santé et de la Recherche Médicale, INSERM U1299 "Developmental Trajectories and Psychiatry", Université Paris-Saclay, Ecole Normale supérieure Paris-Saclay, CNRS, Centre Borelli, Gif-sur-Yvette, France; [16]AP-HP. Sorbonne Université, Department of Child and Adolescent Psychiatry, Pitié-Salpêtrière Hospital, Paris, France; [17]Psychiatry Department, EPS Barthélémy Durand, Etampes, France; [18]Institute of Medical Psychology and Medical Sociology, University Medical Center Schleswig-Holstein, Kiel University, Kiel, Germany; [19]Department of Child and Adolescent Psychiatry and Psychotherapy, University Medical Centre, Göttingen, Germany; [20]Department of Psychiatry and Neuroimaging Center, Technische Universität Dresden, Dresden, Germany; [21]Department of Psychiatry and Neurosciences, Charité–Universitätsmedizin Berlin, corporate member of Freie Universität BerlinHumboldt-

***For correspondence:** xiaoleilin@fudan.edu.cn (XL); jianfeng64@gmail.com (JF)

Competing interest: See page 15

Funding: See page 16

Sent for Review 07 January 2024
Preprint posted 10 January 2024
Reviewed preprint posted 29 February 2024
Reviewed preprint revised 05 June 2024
Version of Record published 18 October 2024

Reviewing Editor: Murim Choi, Seoul National University, Republic of Korea

Universität zu Berlin, and Berlin Institute of Health, Berlin, Germany; [22]School of Psychology and Global Brain Health Institute, Trinity College Dublin, Dublin, Ireland; [23]Centre for Population Neuroscience and Stratified Medicine (PONS Centre), ISTBI, Fudan University, Shanghai, China; [24]Centre for Population Neuroscience and Stratified Medicine (PONS), Department of Psychiatry and Psychotherapy, Charité Universitätsmedizin, Berlin, Germany; [25]Huashan Institute of Medicine, Huashan Hospital affiliated to Fudan University, Shanghai, China; [26]MOE Frontiers Center for Brain Science, Fudan University, Shanghai, China; [27]Zhangjiang Fudan International Innovation Center, Shanghai, China; [28]Department of Computer Science, University of Warwick, Warwick, United Kingdom

Abstract Structural brain aging has demonstrated strong inter-individual heterogeneity and mirroring patterns with brain development. However, due to the lack of large-scale longitudinal neuroimaging studies, most of the existing research focused on the cross-sectional changes of brain aging. In this investigation, we present a data-driven approach that incorporate both cross-sectional changes and longitudinal trajectories of structural brain aging and identified two brain aging patterns among 37,013 healthy participants from UK Biobank. Participants with accelerated brain aging also demonstrated accelerated biological aging, cognitive decline and increased genetic susceptibilities to major neuropsychiatric disorders. Further, by integrating longitudinal neuroimaging studies from a multi-center adolescent cohort, we validated the 'last in, first out' mirroring hypothesis and identified brain regions with manifested mirroring patterns between brain aging and brain development. Genomic analyses revealed risk loci and genes contributing to accelerated brain aging and delayed brain development, providing molecular basis for elucidating the biological mechanisms underlying brain aging and related disorders.

eLife assessment

Duan et al analyzed brain imaging data in UKBK and divided structural brain aging into two groups, revealing that one group is more vulnerable to aging and brain-related diseases compared to the other group. Such subtyping could be **valuable** and utilized in predicting and diagnosing cognitive decline and neurodegenerative brain disorders in the future. This discovery, supported by **solid** evidence, harbors a substantial impacts in aging and brain structure and function.

Introduction

The structure of the brain undergoes continual changes throughout the entire lifespan, with structural brain alterations intimately linking brain development and brain aging (***Fjell and Walhovd, 2010***; ***Shaw et al., 2008***). Brain aging is a progressive process that often co-occurs with biological aging and declines of cognitive functions (***Elliott et al., 2021***; ***Mattson and Arumugam, 2018***; ***Park and Reuter-Lorenz, 2009***), which contribute to the onset and acceleration of neurodegenerative (***Mariani et al., 2005***) and neuropsychiatric disorders (***Kaufmann et al., 2019***). Studies on healthy brain aging have revealed significant inter-individual heterogeneity in the patterns of neuroanatomical changes (***Raz et al., 2010***; ***Raz and Rodrigue, 2006***). Therefore, examining the patterns of structural brain aging and its associations with cognitive decline is of paramount importance in understanding the diverse biological mechanisms of age-related neuropsychiatric disorders.

Despite the fact that there exist large differences between brain development and brain aging (***Courchesne et al., 2000***), a discernible association between these two processes remains evident. Direct comparisons of brain development and brain aging using structural MRI indicated a 'last in, first out' mirroring pattern, where brain regions develop relatively late during adolescence demonstrated accelerated degeneration in older ages (***McGinnis et al., 2011***; ***Tamnes et al., 2013***). In addition, brain regions with strong mirroring effects showed increased vulnerability to neurodegenerative and neuropsychiatric disorders, including Alzheimer's disease and schizophrenia (***Douaud et al., 2014***).

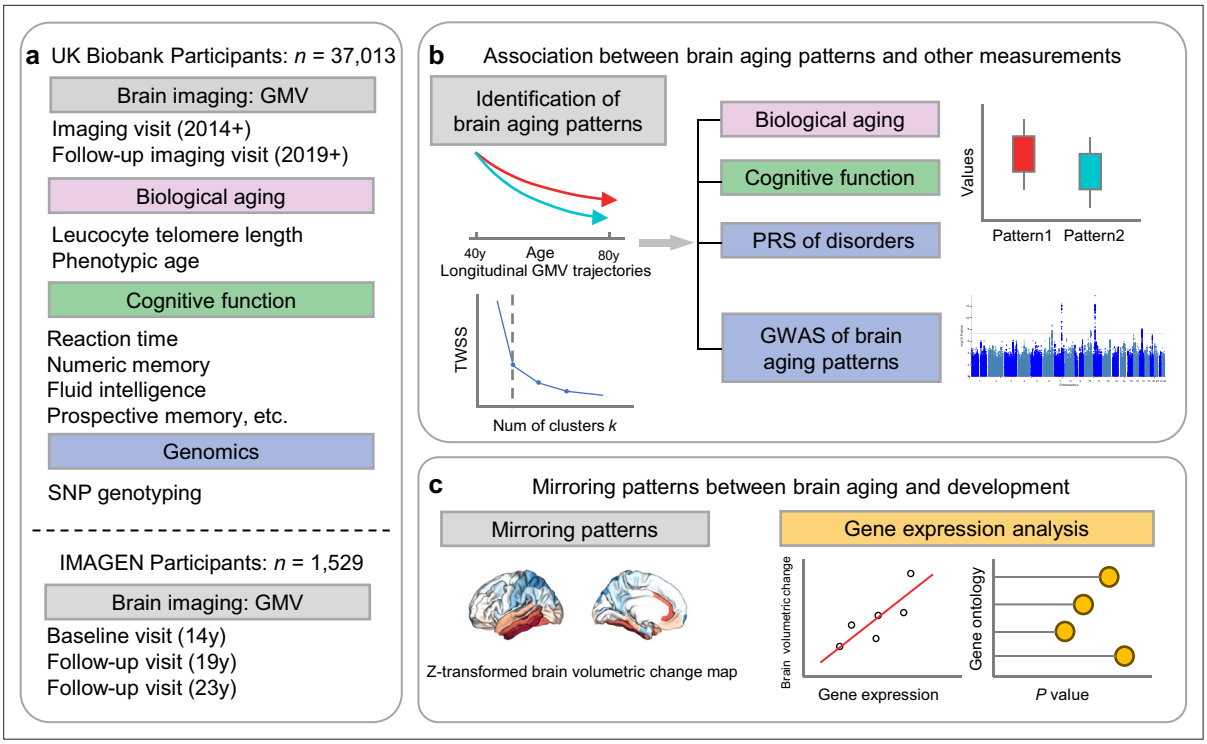

Figure 1. Overview of the study workflow. (**a**) Population cohorts (UK Biobank and IMAGEN) and data sources (brain imaging, biological aging biomarkers, cognitive functions, genomic data) involved in this study. (**b**) Brain aging patterns were identified using longitudinal trajectories of the whole brain GMV, which enabled the capturing of long-term and individualized variations compared to only use cross-sectional data, and associations between brain aging patterns and other measurements (biological aging, cognitive functions and PRS of major neuropsychiatric disorders) were investigated. (c) Mirroring patterns between brain aging and brain development was investigated using z-transformed brain volumetric change map and gene expression analysis.

However, due to the lack of large-scale longitudinal MRI studies during adolescence and mid-to-late adulthood, validation of the 'last in, first out' mirroring hypothesis remains unavailable.

Prior investigations have largely focused on regional and cross-sectional changes of brain aging (***Raz and Rodrigue, 2006***; ***Douaud et al., 2014***; ***Suzuki et al., 2019***), with relatively few studies exploring longitudinal trajectories of brain aging and its associations with brain development (***Raz et al., 2010***; ***Fjell et al., 2015***; ***Nyberg et al., 2023***). In this article, we present a data-driven approach to examine the population clustering of longitudinal brain aging trajectories using structure MRI data obtained from 37,013 healthy individuals during mid-to-late adulthood (44–82 years), and explore its association with biological aging, cognitive decline and susceptibilities for neuropsychiatric disorders. Further, mirroring patterns between longitudinal brain development and brain aging are investigated by comparing the region-specific aging / developmental trajectories, and manifestation of the mirroring patterns are investigated across the whole-brain and among participants with different brain aging patterns. Genomic analyses are conducted to reveal risk loci and genes associated with accelerated brain aging and delayed brain development.

Results

Longitudinal trajectories of whole-brain gray matter volume in mid-to-late adulthood define two brain aging patterns

Figure 1 provides the data sources, analytical workflow and research methodology of this study. After the sample selection process (***Appendix 1—figure 1***, ***Appendix 1—table 1 and 2***), longitudinal grey matter volume (GMV) trajectories in 40 ROIs (33 cortical and 7 subcortical ROIs, see ***Appendix 1—table 3***) were estimated for each of the 37,013 healthy participants in UK Biobank. The first 15 principal components derived from dimensionality reduction via principal component analysis were used

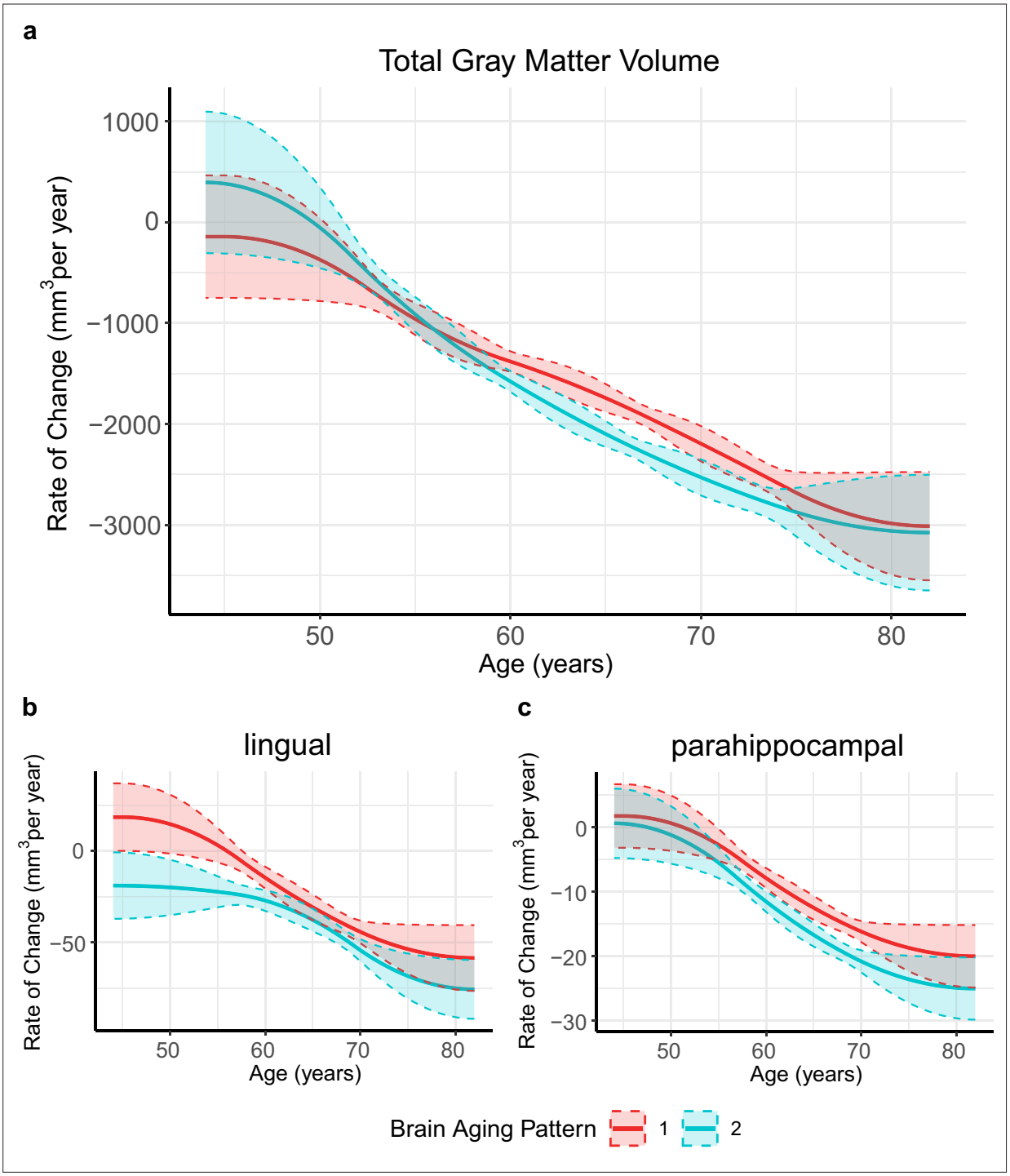

Figure 2. Global (**a**) and selected regional (**b, c**) cortical gray matter volume rate of change among participants with brain aging patterns 1 (red) and 2 (blue). Rates of volumetric change for total gray matter and each ROI were estimated using GAMM, which incorporates both cross-sectional between-subject variation and longitudinal within-subject variation from 40,921 observations and 37,013 participants. Covariates include sex, assessment center, handedness, ethnic, and ICV. Shaded areas around the fit line denotes 95% CI.

The online version of this article includes the following source data for figure 2:

Source data 1. Related to ***Figure 2***.

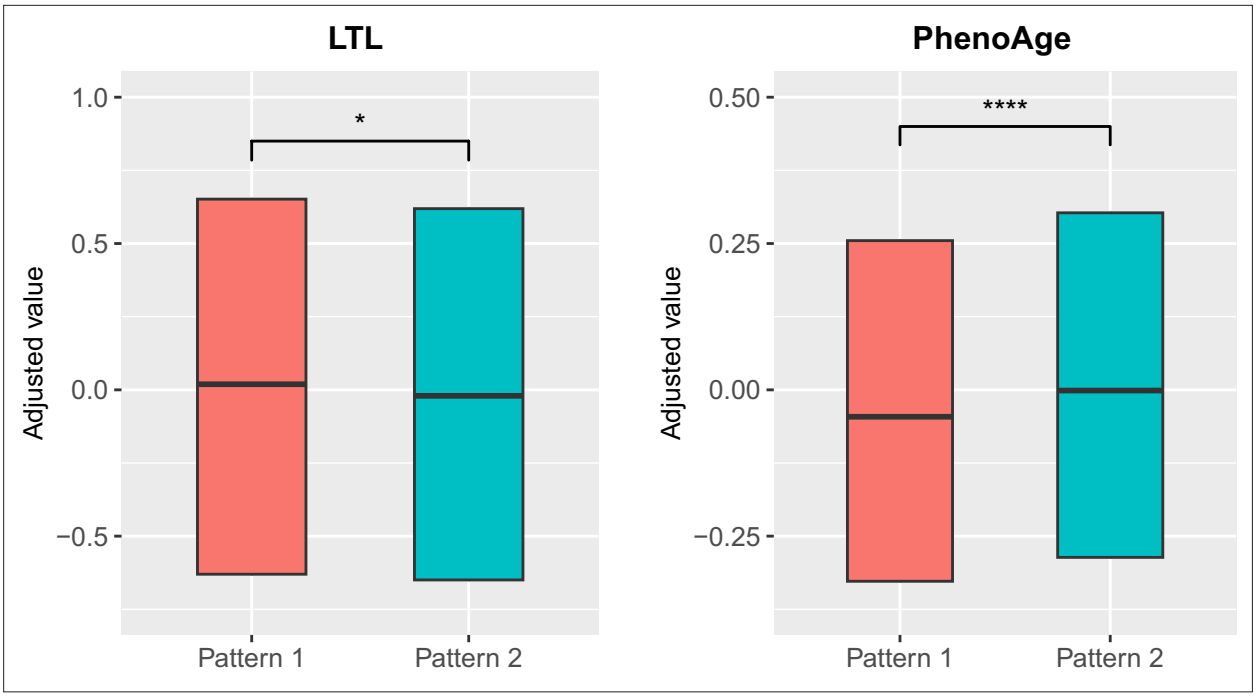

Figure 3. Distributions of biological aging biomarkers (leucocyte telomere length (LTL) and PhenoAge) among participants with brain aging patterns 1 and 2. Boxes represent the interquartile range (IQR), lines within the boxes indicate the median. Two-sided p values were obtained by comparing LTL or PhenoAge ***Levine et al., 2018*** between brain aging patterns using unadjusted multivariate linear regression models. Results remained significant when adjusting for sex, age, ethnic, BMI, smoking status and alcohol intake frequency in the LTL model ***Demanelis et al., 2020*** and sex, age, ethnic, BMI, smoking status, alcohol frequency and education years in PhenoAge model. Stars indicate statistical significance after Bonferroni correction. ****: $p \leq 0.0001$, *: $p \leq 0.05$.

The online version of this article includes the following source data for figure 3:

Source data 1. Related to ***Figure 3***.

in the clustering analysis (see Methods; ***Alexander-Bloch et al., 2013***; ***Whitwell et al., 2009***). Two brain aging patterns were identified, where 18,929 (51.1%) participants with the first brain aging pattern (pattern 1) had higher total GMV at baseline and a slower rate of GMV decrease over time, and the remaining participants with the second pattern (pattern 2) had lower total GMV at baseline and a faster rate of GMV decrease (***Figure 2a***). Comparing the region-specific rate of GMV decrease, pattern 2 showed a more rapid GMV decrease in medial occipital (lingual gyrus, cuneus, and pericalcarine cortex) and medial temporal (entorhinal cortex, parahippocampal gyrus) regions (***Figure 2b and c*** and ***Appendix 1—figure 2***), which had the largest loadings in the second and third principal components (***Appendix 1—table 4***). These two patterns can be clearly stratified by both linear and non-linear dimensionality reduction methods, indicating distinct structural differences in brain aging between patterns (***Appendix 1—figure 3***). Sample characteristics of these 37,013 UK Biobank participants stratified by brain aging patterns are summarized in ***Appendix 1—table 5***. Overall, participants with different brain aging patterns had similar distributions with regard to age, sex, ethnicity, smoking status, Townsend deprivation index (TDI), body mass index (BMI) and years of schooling.

Brain aging patterns were significantly associated with biological aging

To explore the relationships between structural brain aging and biological aging, we investigated the distribution of aging biomarkers, such as telomere length and PhenoAge (***Levine et al., 2018***), across brain aging patterns identified above (***Figure 3*** and ***Appendix 1—table 6***). Compared to pattern 1, participants in pattern 2 with more rapid GMV decrease had shorter leucocyte telomere length (p=0.009, Cohen's D=–0.028) and this association remained consistent after adjusting for sex, age, ethnic, BMI, smoking status and alcohol intake frequency (***Demanelis et al., 2020***). Next, we examined PhenoAge, which was developed as an aging biomarker incorporating composite clinical and biochemical data (***Levine et al., 2018***), and observed higher PhenoAge among participants with

brain aging pattern 2 compared to pattern 1 (p=0.019, Cohen's D=0.027). Again, the association remained significant after adjusting for sex, age, ethnic, BMI, smoking status, alcohol intake frequency and education years ($p=3.05\times10^{-15}$, Cohen's D=0.092). Group differences in terms of each individual component of PhenoAge (including albumin, creatinine, glucose, c-reactive protein, lymphocytes percentage, mean corpuscular volume, erythocyte distribution width, alkaline phosphatase and leukocyte count) were also investigated and results were consistent with PhenoAge (***Appendix 1—figure 4***).

Accelerated brain aging was associated with cognitive decline and increased genetic susceptibilities to attention-deficit/hyperactivity disorder and delayed brain development

Next, we conducted comprehensive comparisons of cognitive functions between participants with different brain aging patterns. In general, those with brain aging pattern 2 (lower baseline total GMV and more rapid GMV decrease) exhibited worse cognitive performances compared to pattern 1. Specifically, brain aging pattern 2 showed lower numbers of correct pairs matching (p=0.006, Cohen's D=–0.029), worse prospective memory (OR = 0.943, 95% CI [0.891, 0.999]), lower fluid intelligence ($p<1.00\times10^{-20}$, Cohen's D=–0.102), and worse numeric memory ($p=5.97\times10^{-11}$, Cohen's D=–0.082). No statistically significant differences were observed in terms of the reaction time (p=0.99) and

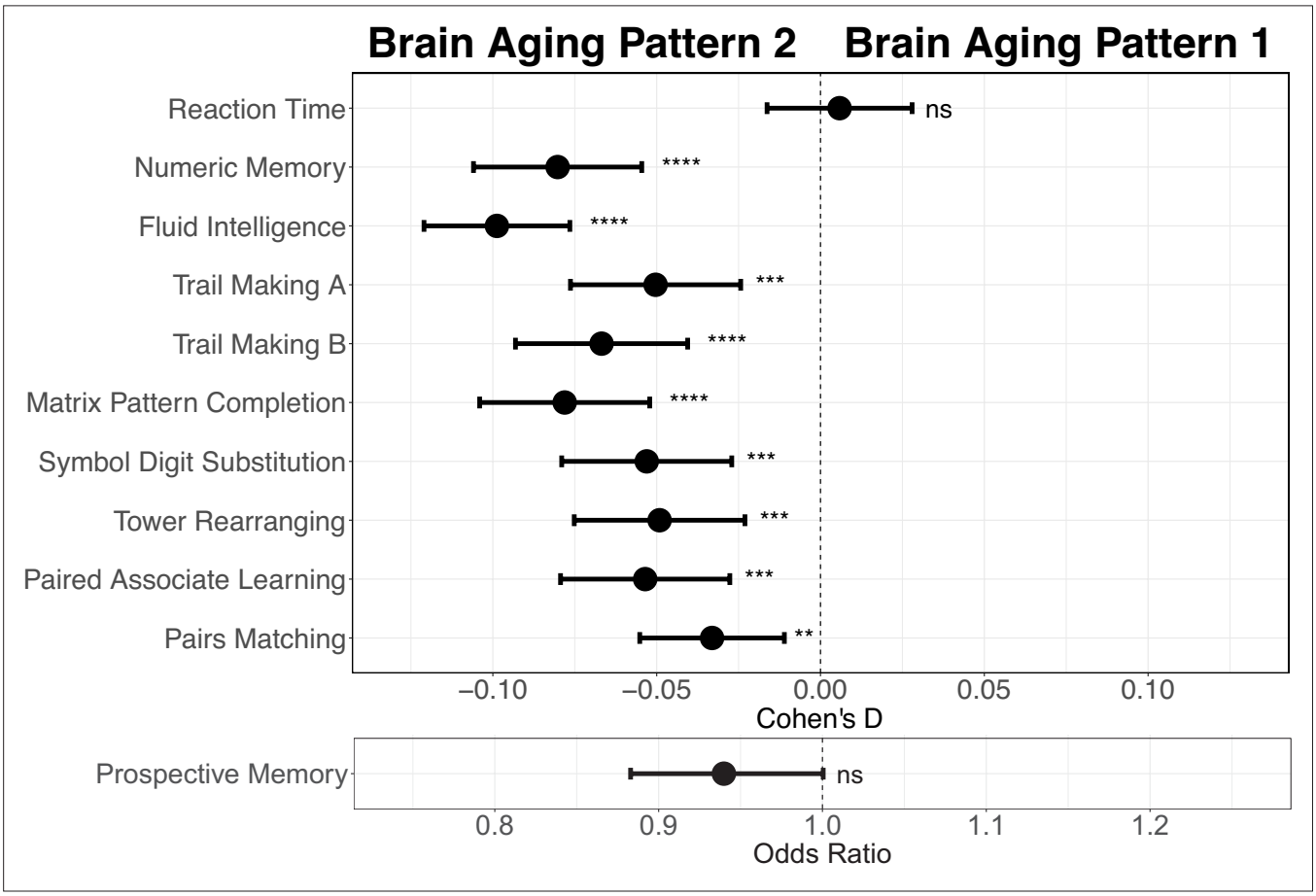

Figure 4. Effect size (Cohen's D or odds ratio) for comparing the cognitive functions between participants with brain aging patterns 1 and 2. Results were adjusted such that negative Cohen's D and Odds Ratio less than 1 indicate worse cognitive performances in brain aging pattern 2 compared to pattern 1. Width of the lines extending from the center point represent 95% confidence interval. Two-sided p values were obtained using both unadjusted and adjusted (for sex, age, and TDI, education and income) multivariate regression models. Stars indicate statistical significance after FDR correction for 11 comparisons. ****: $p \le 0.0001$, ***: $p \le 0.001$, **: $p \le 0.01$, ns: $p>0.05$.

The online version of this article includes the following source data for figure 4:

Source data 1. Related to ***Figure 4***.

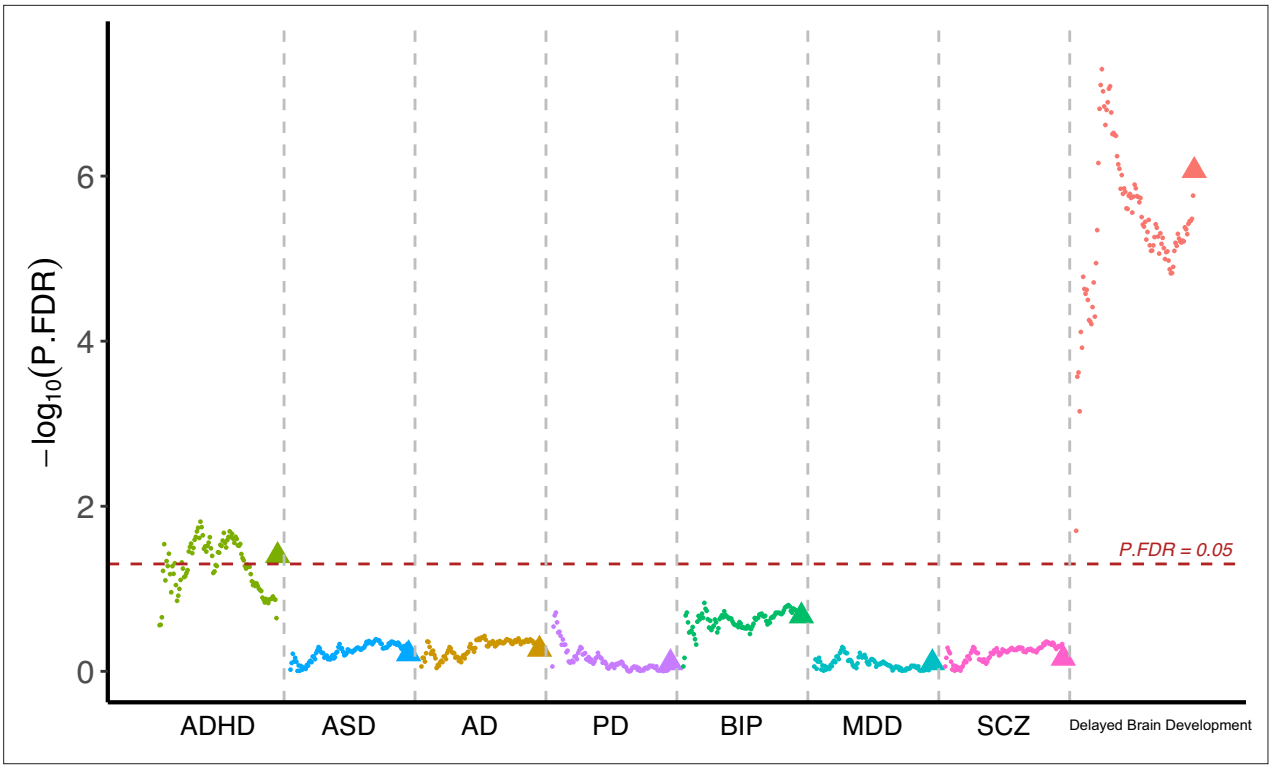

Figure 5. Participants with accelerated brain aging (brain aging pattern 2) had significantly increased genetic liability to ADHD and delayed brain development. Polygenic risk score (PRS) for ADHD, ASD, AD, PD, BIP, MDD, SCZ and delayed brain development (unpublished GWAS) were calculated at different p-value thresholds from 0.005 to 0.5 at an interval of 0.005. Vertical axis represents negative logarithm of P values comparing PRS in brain aging pattern 2 relative to pattern 1. Red horizontal dashed line indicates FDR corrected p value of 0.05. Colors represent traits and dots within the same color represent different p value thresholds. The trigonometric symbol indicates the average PRS across all p-value thresholds for the same trait.

The online version of this article includes the following source data for figure 5:

Source data 1. Related to ***Figure 5***.

prospective memory (p=0.052) between these two brain aging patterns after FDR correction. Results were consistent when using models adjusted for sex, age, and socioeconomic status (TDI, education and income; ***Foster et al., 2018***; ***Townsend et al., 2023***; ***Figure 4***). Full results demonstrating the associations between brain aging patterns and cognitive functions are presented in ***Appendix 1—table 7***.

Having observed cognitive decline among participants with accelerated brain aging pattern, we next investigated whether brain aging patterns were associated with genetic vulnerability to major neuropsychiatric disorders. Since current GWAS are under-powered for attention-deficit/hyperactivity disorder (ADHD) and autism spectrum disorders (ASD) and the difficulty in identifying genetic variants was likely due to their polygenic nature, we calculated the corresponding polygenic risk scores (PRS) using multiple p value thresholds. This approach enabled robust investigation of the association between genetic susceptibility of neuropsychiatric disorders and brain imaging phenotypes. PRS for major neuro-developmental disorders including attention-deficit/hyperactivity disorder (ADHD) and autism spectrum disorders (ASD), neurodegenerative diseases including Alzheimer's disease (AD) and Parkinson's disease (PD), neuropsychiatric disorders including bipolar disorder (BIP), major depressive disorder (MDD), and schizophrenia (SCZ), and delayed structural brain development (GWAS from an unpublished longitudinal neuroimaging study) (***Shi et al., 2023***) were calculated for each participant using multiple p value thresholds (from 0.005 to 0.5 at intervals of 0.005) and results were then averaged over all thresholds (***Figure 5***). The primary GWAS datasets used for calculating the PRS were listed in ***Appendix 1—table 8***. Overall, we observed increased genetic susceptibility to ADHD (p=0.040) and delayed brain development ($p=1.48\times10^{-6}$) among participants with brain aging pattern 2 after FDR correction, while no statistically significant differences were observed for ASD, AD, PD,

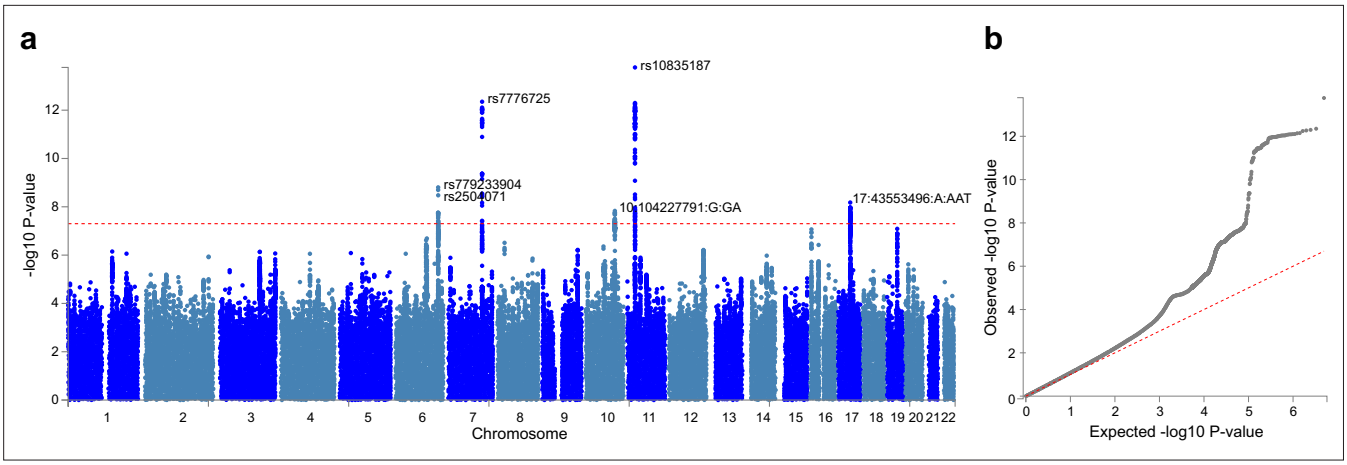

Figure 6. Genome-wide association study (GWAS) identified 6 independent SNPs associated with accelerated brain aging. Total GMV at 60 years old was estimated for each participant using mixed effect models allowing for individualized baseline GMV and GMV change rate, and was used as the phenotype in the GWAS. (**a**) At genome-wide significance level ($p=5\times10^{-8}$, red dashed line), rs10835187 and rs7776725 loci were identified to be associated with accelerated brain aging. (**b**) Quantile–quantile plot showed that the most significant p values deviate from the null, suggesting that results are not unduly inflated.

BIP, MDD, and SCZ (***Figure 5***). Details regarding the genetic liability to other common diseases and phenotypes using enhanced PRS from UK Biobank are displayed in ***Appendix 1tables 9 and 10***.

Genome Wide Association Studies (GWAS) identified significant genetic loci associated with accelerated brain aging

Having observed significant associations between brain aging patterns and cognitive performances / genetic liabilities to major neurodevelopmental disorders, we further investigated if there exist genetic variants contributing to individualized brain aging phenotype. We conducted genome-wide association studies (GWAS) using estimated total GMV at 60 years old as the phenotype. This phenotype was derived by adding individual specific deviations to the population averaged total GMV, thus providing additional information compared to studies using only cross-sectional neuroimaging phenotypes.

Six independent single nucleotide polymorphisms (SNPs) were identified at genome-wide significance level ($p<5\times10^{-8}$) (***Figure 6***) and were subsequently mapped to genes using NCBI, Ensembl and UCSC Genome Browser database (***Appendix 1—table 11***). Among them, two SNPs (rs10835187 and rs779233904) were also found to be associated with multiple brain imaging phenotypes in previous studies (***Smith et al., 2021***), such as regional and tissue volume, cortical area and white matter tract measurements. Compared to the GWAS using global gray matter volume as the phenotype, our GWAS revealed additional signal in chromosome 7 (rs7776725), which was mapped to the intron of FAM3C and encodes a secreted protein involved in pancreatic cancer (***Grønborg et al., 2006***) and Alzheimer's disease (***Liu et al., 2016***). This signal was further validated to be associated with specific brain aging mode by another study using a data-driven decomposition approach (***Smith et al., 2020***). In addition, another significant loci (rs10835187, $p=1.11\times10^{-13}$) is an intergenic variant between gene LGR4-AS1 and LIN7C, and was reported to be associated with bone density and brain volume measurement (***Smith et al., 2021***; ***Estrada et al., 2012***). *LIN7C* encodes the Lin-7C protein, which is involved in the localization and stabilization of ion channels in polarized cells, such as neurons and epithelial cells (***Bohl et al., 2007***; ***Kaech et al., 1998***). Previous study has revealed the association of both allelic and haplotypic variations in the *LIN7C* gene with ADHD (***Lanktree et al., 2008***).

Mirroring patterns between brain aging and brain development

Having observed significant associations between brain aging and genetic susceptibility to neurodevelopmental disorders, we are now interested in examining the mirroring patterns between brain aging and brain development in the whole population, and whether these mirroring patterns were more pronounced in those with accelerated brain aging. Adolescents in the IMAGEN cohort showed

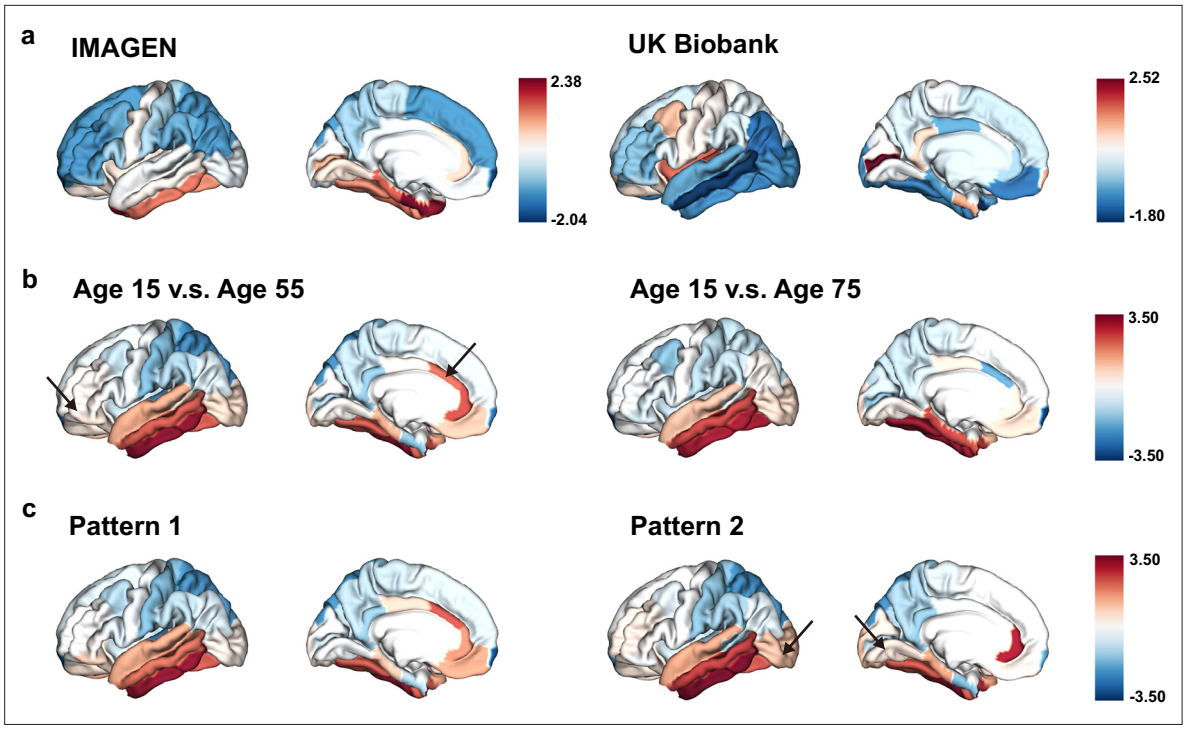

Figure 7. The 'last in, first out' mirroring patterns between brain development and brain aging. (**a**) The annual percentage volume change (APC) was calculated for each ROI and standardized across the whole brain in adolescents (IMAGEN, left) and mid-to-late aged adults (UK Biobank, right), respectively. For adolescents, ROIs of in red indicate delayed structural brain development, while for mid-to-late aged adults, ROIs in blue indicate accelerated structural brain aging. (**b**) Estimated APC in brain development versus early aging (55 years old, left), and versus late aging (75 years old, right). ROIs in red indicate faster GMV decrease during brain aging and slower GMV decrease during brain development, that is stronger mirroring effects between brain development and brain aging. (**c**) Mirroring patterns between brain development and brain aging were more manifested in participants with accelerated aging (brain aging pattern 2). The arrows point to ROIs with more pronounced mirroring patterns in each subfigure.

The online version of this article includes the following source data for figure 7:

Source data 1. Related to ***Figure 7***.

more rapid GMV decrease in the frontal and parietal lobes, especially the frontal pole, superior frontal gyrus, rostral middle frontal gyrus, inferior parietal lobule and superior parietal lobule, while those in their mid-to-late adulthood showed more accelerated GMV decrease in the temporal lobe, including medial orbitofrontal cortex, inferior parietal lobule and lateral occipital sulcus (***Figure 7a***). The mirroring patterns (with slower GMV decrease during brain development and more rapid GMV decrease during brain aging) were particularly prominent in inferior temporal gyrus, caudal anterior cingulate cortex, fusiform cortex, middle temporal gyrus and rostral anterior cingulate cortex (***Figure 7b***). The regional mirroring patterns became weaker when we focus on late brain aging at age 75 years old, especially in the frontal lobe and cingulate cortex. Further, mirroring patterns were represented more prominently in participants with brain aging pattern 2, where stronger mirroring between brain aging and brain development was observed in frontotemporal area, including lateral occipital sulcus and lingual gyrus (***Figure 7c***).

Gene expression profiles were associated with delayed brain development and accelerated brain aging

The Allen Human Brain Atlas (AHBA) transcriptomic dataset (http://human.brain-map.org) were used to obtain the spatial correlation between gene expression profiles across cortex and structural brain development/aging via partial least square (PLS) regression. The first PLS component explained 24.7% and 53.6% of the GMV change during brain development (estimated at age 15y, $r_{spearman}$ = 0.51, $P_{permutation}$ = 0.03) and brain aging (estimated at age 55y, $r_{spearman}$ = 0.49, $P_{permutation}$ = 1.5×10^{-4}), respectively. Seventeen of the 45 genes mapped to GWAS significant SNP were found in AHBA, with *LGR4* ($r_{spearman}$ = 0.56, $P_{permutation}$ <0.001) significantly associated with delayed brain development and *ESR1* ($r_{spearman}$

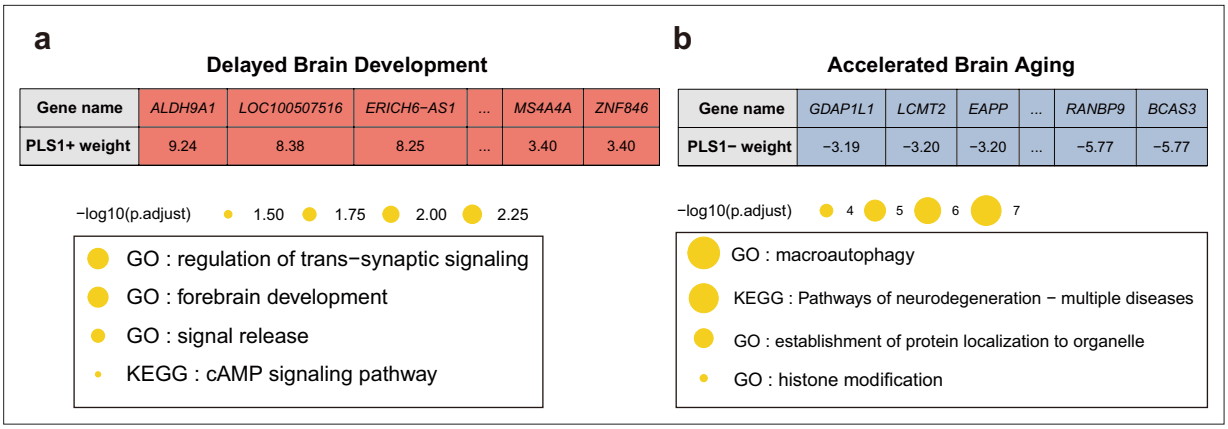

Figure 8. Functional enrichment of gene transcripts significantly associated with delayed brain development and accelerated brain aging. (**a**) 990 genes were spatially correlated with the first PLS component of delayed structural brain development, and were enriched for trans-synaptic signal regulation, forebrain development, signal release and cAMP signaling pathway. (**b**) 2293 genes were spatially correlated the first PLS component of accelerated structural brain aging, and were enriched for macroautophagy, pathways of neurodegeneration, establishment of protein localization to organelle and histone modification. Size of the circle represents number of genes in each term and P values were corrected using FDR for multiple comparisons.

The online version of this article includes the following source data for figure 8:

Source data 1. Related to ***Figure 8***.

Source data 2. Related to ***Figure 8***.

= 0.53, $P_{permutation}$ <0.001) and *FAM3C* ($r_{spearman}$ = –0.37, $P_{permutation}$ = 0.004) significantly associated with accelerated brain aging. *BDNF-AS* was positively associated with both delayed brain development and accelerated brain aging after spatial permutation test (***Appendix 1—table 12 and 13***).

Next, we screened the genes based on their contributions and effect directions to the first PLS components in brain development and brain aging. 990 and 2293 genes were identified to be positively associated with brain development and negatively associated with brain aging at FDR corrected p value of 0.005, respectively, representing gene expressions associated with delayed brain development and accelerated brain aging. These genes were then tested for enrichment of GO biological processes and KEGG pathways. Genes associated with delayed brain development showed significant enrichment in 'regulation of trans-synaptic signaling', 'forebrain development', 'signal release' and 'cAMP signaling pathway' (***Figure 8a***), and genes associated with accelerated brain aging showed significant enrichment in 'macroautophagy', 'establishment of protein localization to organelle', 'histone modification', and 'pathways of neurodegeneration – multiple diseases' (***Figure 8b***). Full results of the gene set enrichment analysis were provided in ***Appendix 1—figure 5***. In summary, the analyses from using the databases of GO biological processes and KEGG Pathways indicate synaptic transmission as an important process in the common mechanisms of brain development and aging, and cellular processes (autophagy), as well as the progression of neurodegenerative diseases, are important processes in the mechanisms of brain aging.

Discussion

In this study, we adopted a data-driven approach and revealed two distinct brain aging patterns using large-scale longitudinal neuroimaging data in mid-to-late adulthood. Compared to brain aging pattern 1, brain aging pattern 2 were characterized by a faster rate of GMV decrease, accelerated biological aging, cognitive decline, and genetic susceptibility to neurodevelopmental disorders. By integrating longitudinal neuroimaging data from adult and adolescent cohorts, we demonstrated the 'last in, first out' mirroring patterns between structural brain aging and brain development, and showed that the mirroring pattern was manifested in the temporal lobe and among participants with accelerated brain aging. Further, genome-wide association studies identified significant genetic loci contributing to accelerated brain aging, while spatial correlation between whole-brain transcriptomic profiles and structural brain aging / development revealed important gene sets associated with both accelerated brain aging and delayed brain development.

Brain aging is closely related to the onset and progression of neurodegenerative and neuropsychiatric disorders. Both neurodegenerative and neuropsychiatric disorders demonstrate strong inter-individual heterogeneity, which prevents the comprehensive understanding of their neuropathology and neurogenetic basis. Therefore, multidimensional investigation into disease subtyping and population clustering of structural brain aging are crucial in elucidating the sources of heterogeneity and neurophysiological basis related to the disease spectrum (***Habes et al., 2020***). In the last decades, major developments in the subtyping of Alzheimer's disease, dementia and Parkinson's disease, have provided new perspectives regarding their clinical diagnosis, treatment, disease progression and prognostics (***Habes et al., 2020***; ***Berg et al., 2021***; ***Ferreira et al., 2020***). While previous studies of brain aging mostly focused on the cross-sectional differences between cases and healthy controls, we here delineated the structural brain aging patterns among healthy participants using a novel data-driven approach that captured both cross-sectional and longitudinal trajectories of the whole-brain gray matter volume (***Feczko et al., 2019***; ***Poulakis et al., 2022***). The two brain aging patterns identified using the above approach showed large differences in the rate of change in medial occipitotemporal gyrus, which is involved in vision, word processing, and scene recognition (***Bogousslavsky et al., 1987***; ***Epstein et al., 1999***; ***Mechelli et al., 2000***). Significant reduction of the gray matter volume and abnormal changes of the functional connectivity in this region were found in subjects with mild cognitive impairment (MCI) and AD, respectively (***Chételat et al., 2005***; ***Yao et al., 2010***). Previous research on brainAGE (***Elliott et al., 2021***; ***Christman et al., 2020***) (the difference between chronological age and the age predicted by the machine learning model of brain imaging data) showed that as a biomarker of accelerated brain aging, people with older brainAGE have accelerated biological aging and early signs of cognitive decline, which is consistent with our discoveries in this study. Our results support the establishment of a network connecting brain aging patterns with biological aging profiles involving multi-organ systems throughout the body (***Tian et al., 2023***). Since structural brain patterns might manifest and diverge decades before cognitive decline (***Aljondi et al., 2019***), subtyping of brain aging patterns could aid in the early prediction of cognitive decline and severe neurodegenerative and neuropsychiatric disorders.

Mirroring pattern between brain development and brain aging has long been hypothesized by postulating that phylogenetically newer and ontogenetically less precocious brain structures degenerate relatively early (***Douaud et al., 2014***). Early studies have reported a positive correlation between age-related differences of cortical volumes and precedence of myelination of intracortical fibers (***Raz, 2000***). Large differences in the patterns of change between adolescent late development and aging in the medial temporal cortex were previously found in studies of brain development and aging patterns (***Tamnes et al., 2013***). Here, we compared the annual volume change of the whole-brain gray matter during brain development and early / late stages of brain aging, and found that mirroring patterns are predominantly localized to the lateral / medial temporal cortex and the cingulate cortex. These cortical regions characterized by 'last in, first out' mirroring patterns showed increased vulnerability to the several neuropsychiatric disorders. For example, regional deficits in the superior temporal gyrus and medial temporal lobe were observed in schizophrenia (***Honea et al., 2005***), along with morphological abnormalities in the medial occipitotemporal gyrus (***Schultz et al., 2010***). Children diagnosed with ADHD had lower brain surface area in the frontal, cingulate, and temporal regions (***Hoogman et al., 2019***). ***Douaud et al., 2014*** revealed a population transmodal network with lifespan trajectories characterized by the mirroring pattern of development and aging. We investigated the genetic susceptibility to individual-level mirroring patterns based on the lasting impact of neurodevelopmental genetic factors on brain (***Fjell et al., 2015***), demonstrating that those with more rapidly brain aging patterns have a higher risk of delayed development.

Identifying genes contributing to structural brain aging remains a critical step in understanding the molecular changes and biological mechanisms that govern age-related cognitive decline. Several genetic loci have been reported to be associated with brain aging modes and neurocognitive decline, many of which demonstrated global overlap with neuropsychiatric disorders and their related risk factors (***Smith et al., 2020***; ***Glahn et al., 2013***; ***Brouwer et al., 2022***). Here, we focused on the individual brain aging phenotype by estimating individual deviation from the population averaged total GMV and conducted genome-wide association analysis with this phenotype. Our approach identified six risk SNPs associated with accelerated brain aging, most of which could be further validated by previous studies using population averaged brain aging phenotypes. However, our approach revealed

additional genetic signals and demonstrated genetic architecture underlying brain aging patterns overlap with bone density (***Estrada et al., 2012***; ***Zheng et al., 2015***). In addition, molecular profiling of the aging brain has been thoroughly investigated among patients with neurogenerative diseases, but rarely conducted to shed light on the mirroring patterns among healthy participants. Analysis of the spatial correlation between gene expression profiles and structural brain development / aging further identified genes contributing to delayed brain development and accelerated brain aging. Specifically, expression of gene *BDNF-AS* was significantly associated with both processes. *BDNF-AS* is an antisense RNA gene and plays a role in the pathoetiology of non-neoplastic conditions mainly through the mediation of *BDNF* (***Ghafouri-Fard et al., 2021***). LGR4 (associated with delayed brain development) and FAM3C (associated with accelerated brain aging) identified in the spatial genetic association analysis also validated our findings in the GWAS.

There are several limitations in the current study that need to be addressed in future research. Firstly, the UK Biobank cohort, which we leveraged to identify population clustering of brain aging patterns, had a limited number of repeated structural MRI scans. Therefore, it remains challenging to obtain robust estimation of the longitudinal whole-brain GMV trajectory at the individual level. As a robustness check, we have calculated both intra-class correlation and variance of both random intercept and age slope to ensure appropriateness of the mixed effect models. Secondly, although aging is driven by numerous hallmarks, we have only investigated the association between brain aging patterns and biological aging in terms of telomere length and blood biochemical markers due to limitations of data access. Other dimensions of aging hallmarks and their relationship with structural brain aging need to be investigated in the future. Thirdly, our genomic analyses were restricted to 'white British' participants of European ancestry. The diversity of genomic analyses will continue to improve as the sample sizes of GWAS of non-European ancestry increase. Further, although the gene expression maps from Allen Human Brain Atlas enabled us to gain insights into the spatial coupling between gene expression profiles and mirroring patterns of the brain, the strong inter-individual variation of whole-brain gene expression levels and large temporal span of the human brain samples may lead to the inaccurate correspondence in the observed associations. Finally, we focused on structural MRIs in deriving brain aging patterns in this analysis, future investigations could consider other brain imaging modalities from a multi-dimensional perspective. Nevertheless, our study represents a novel attempt for population clustering of structural brain aging and validated the mirroring pattern hypothesis by leveraging large-scale adolescent and adult cohorts.

Methods

Participants

T1-weighted brain MRI images were obtained from 37,013 individuals aged 44–82 years old from UK Biobank (36,914 participants at baseline visit in 2014+, 4007 participants at the first follow-up visit in 2019+). All participants from UK Biobank provided written informed consent, and ethical approval was granted by the North West Multi-Center Ethics committee (https://www.ukbiobank.ac.uk/learn-more-about-uk-biobank/about-us/ethics) with research ethics committee (REC) approval number 16/NW/0274. Participants were excluded if they were diagnosed with severe psychiatric disorders or neurological diseases using ICD-10 primary and secondary diagnostic codes or from self-reported medical conditions at UK Biobank assessment center (see ***Appendix 1—tables 1 and 2***). Data were obtained under application number 19542. A total of 1529 adolescents with structural MRI images were drawn from the longitudinal project IMAGEN (1463 at age 14, 1377 at age 19, and 1148 at age 23), of which the average number of MRI scans was 2.61 per adolescent. The IMAGEN study was approved by local ethics research committees of King's College London, University of Nottingham. Trinity College Dublin, University of Heidelberg, Technische Universität Dresden, Commissariat à l'Énergie Atomique et aux Énergies Alternatives, and University Medical Center at the University of Hamburg in compliance with the Declaration of Helsinki (***Association, 2013***). Informed consent was given by all participants and a parent/guardian of each participant.

MRI acquisition

Quality-controlled T1-weighted neuroimaging data from UK Biobank and IMAGEN were processed using FreeSurfer v6.0. Detailed imaging processing pipeline can be found online for UK Biobank

(https://biobank.ctsu.ox.ac.uk/crystal/crystal/docs/brain_mri.pdf) and IMAGEN (https://github.com/imagen2/imagen_mri; ***Schumann et al., 2010***; ***Imagen, 2020***). Briefly, cortical gray matter volume (GMV) from 33 regions in each hemisphere were generated using Desikan–Killiany Atlas (***Desikan et al., 2006***), and total gray matter volume (TGMV), intracranial volume (ICV) and subcortical volume were derived from ASEG atlas (***Fischl et al., 2002*** See ***Appendix 1—table 3***). Regional volume was averaged across left and right hemispheres. To avoid deficient segmentation or parcellation, participants with TGMV, ICV or regional GMV beyond 4 standard deviations from the sample mean were considered as outliers and removed from the following analyses.

Identification of longitudinal brain aging patterns

Whole-brain GMV trajectory was estimated for each participant in 40 brain regions of interest (ROIs) (33 cortical regions and 7 subcortical regions), using mixed effect regression model with fixed linear and quadratic age effects, random intercept and random age slope. Covariates include sex, assessment center, handedness, ethnic, and ICV. Models with random intercept and with both random intercept and random age slope were compared using AIC, BIC and evaluation of intra-class correlation (ICC). Results suggested that random age slope model should be chosen for almost all ROIs (***Appendix 1—table 14***). Deviation of regional GMV from the population average was calculated for each participant at age 60 years and dimensionality reduction was conducted via principal component analysis (PCA). The first 15 principal components explaining approximately 70% of the total variations of regional GMV deviation were used in multivariate k-means clustering. Optimal number of clusters was chosen using both elbow diagram and contour coefficient (***Appendix 1—figure 6***). Rates of volumetric change for total gray matter and each ROI were estimated using generalized additive mixed effect models (GAMM) with fixed cubic splines of age, random intercept and random age slope, which incorporates both cross-sectional between-subject variation and longitudinal within-subject variation from 40,921 observations and 37,013 participants. Covariates include sex, assessment center, handedness, ethnic, and ICV. We also applied PCA and locally linear embedding (LLE; ***Roweis and Saul, 2000***) to the adjusted GMV ROIs in order to map the high-dimensional imaging-derived phenotypes to a low-dimensional space for stratification visualisation. The GMV of 40 ROIs at baseline were linearly adjusted for sex, assessment center, handedness, ethnic, ICV, and second-degree polynomial in age to be consistent with the whole-brain GMV trajectory model.

Association between brain aging patterns and biological aging, cognitive decline and genetic susceptibilities of neuropsychiatric disorders

Individuals with Z-standardized leucocyte telomere length (***Codd et al., 2021***) and blood biochemistry (which were used to calculate PhenoAge (***Levine et al., 2018***) that characterizes biological aging) outside 4 standard deviations from the sample mean were excluded for better quality control. A total of 11 cognitive tests performed on the touchscreen questionnaire were included in the analysis. More information about the cognitive tests is provided in Supplementary Information. Comparisons of biological aging (leucocyte telomere length, PhenoAge) and cognitive function were conducted among participants with different brain aging patterns using both unadjusted and adjusted multivariate regression models with Bonferroni / FDR correction. Polygenic Risk Scores (PRS) were calculated for autism spectrum disorder (ASD), attention deficit hyperactivity disorder (ADHD), Alzheimer's disease (AD), Parkinson's Disease (PD), bipolar disorder (BIP), major depressive disorder (MDD), schizophrenia (SCZ), and delayed brain development using GWAS summary statistics (***Shi et al., 2023***) at multiple p value thresholds (from 0.005 to 0.5 at intervals of 0.005, and 1), with higher p value thresholds incorporating larger number of independent SNPs. After quality control of genotype and imaging data, PRSs were generated for 25,861 participants on UK Biobank genotyping data. SNPs were pruned and clumped with a cutoff $r^2 \geq 0.1$ within a 250 kb window. All calculations were conducted using PRSice v2.3.5 (***Choi and O'Reilly, 2019***). Enhanced PRS from UK Biobank Genomics for multiple diseases were also tested. Detailed instructions for calculating enhanced PRS in UK Biobank can be found in research of ***Thompson et al., 2022*** Comparisons of neuropsychiatric disorders were conducted among participants with different brain aging patterns using t test with FDR correction. All statistical tests were two-sided.

Genome wide association Study to identify SNPs associated with brain aging patterns

We performed Genome-wide association studies (GWAS) on individual deviations of total GMV relative to the population average at 60 years using PLINK 2.0 (***Chang et al., 2015***). Variants with missing call rates exceeding 5%, minor allele frequency below 0.5% and imputation INFO score less than 0.8 were filtered out after the genotyping quality control for UK Biobank Imputation V3 dataset. Among the 337,138 unrelated 'white British' participants of European ancestry included in our study, 25,861 with recent UK ancestry and accepted genotyping and imaging quality control were included in the GWAS. The analyses were further adjusted for age, age2, sex, assessment center, handedness, ethnic, ICV, and the first 10 genetic principal components. Genome-wide significant SNPs ($p<5\times10^{-8}$) obtained from the GWAS were clumped by linkage disequilibrium (LD) (r^2 <0.1 within a 250 kb window) using UKB release2b White British as the reference panel. We subsequently performed gene-based annotation in FUMA (***Watanabe et al., 2017***) using genome-wide significant SNPs and SNPs in close LD ($r^2 \geq 0.1$) using Annotate Variation (ANNOVAR) on Ensemble v102 genes (***Wang et al., 2010***).

Mirroring patterns between brain aging and brain development

To validate the 'last in, first out' mirroring hypothesis, we evaluated the structural association between brain development and brain aging. Longitudinal neuroimaging data from 1529 adolescents in the IMGAEN cohort and 3908 mid-to-late adulthood in the UK Biobank cohort were analyzed. Annual percentage volume change (APC) for each ROI was calculated among individuals with at least two structural MRI scans by subtracting the baseline GMV from follow-up GMV and dividing by the number of years between baseline and follow-up visits. Region-specific APC was regressed on age using smoothing spline with cross validated degree of freedom. Estimated APC for each ROI was obtained at age 15y for adolescents and at age 55y (early aging) and 75y (late aging) for participants in UK Biobank. Region-specific APC during adolescence (or mid-to-late adulthood) was then standardized across all cortical regions to create the brain development (or aging) map. Finally, the brain development map and brain aging map were compared to assess the mirroring pattern for each ROI in the overall population and across different aging subgroups.

Gene expression analysis

The Allen Human Brain Atlas (AHBA) dataset (http://human.brain-map.org), which comprises gene expression measurements in six postmortem adults (age 24–57y) across 83 parcellated brain regions (***Hawrylycz et al., 2012***; ***Markello et al., 2021***), were used to identify gene expressions significantly associated with structural brain development and aging. The expression profiles of 15,633 genes were averaged across donors to form a 83×15,633 transcriptional matrix and partial least squares (PLS) regression was adopted for analyzing the association between regional change rate of gray matter volume and gene expression profiles. Specifically, estimated regional APC at 15 (obtained from IMAGEN cohort) and 55 years old (obtained from UK Biobank) were regressed on the high-dimensional gene expression profiles upon regularization. Associations between the first PLS component and estimated APC during brain development and brain aging were tested by spatial permutation analysis (10,000 times; ***Váša et al., 2018***). Additionally, gene expression profiles of genes mapped to GWAS significant SNP were extracted from AHBA. The association between gene expression profiles of mapped genes and estimated APC during brain development and aging was also tested by spatial permutation analysis. Statistical significance of each gene's contribution to the first PLS component was tested with standard error calculated using bootstrap (***Li et al., 2021***; ***Morgan et al., 2019***; ***Romero-Garcia et al., 2020***), and genes significantly associated with delayed brain development and accelerated brain aging were selected. Enrichment of Kyoto Encyclopedia of Genes and Genomes (KEGG) pathways and gene ontology (GO) of biological processes for these selected genes were analyzed using R package clusterProfiler (***Yu et al., 2012***). All statistical significances were corrected for multiple testing using FDR.

Code availability

R version 4.2.0 was used to perform statistical analyses. FreeSurfer version 6.0 was used to process neuroimaging data. lme4 1.1 in R version 4.2.0 was used to perform longitudinal data analyses. PRSice version 2.3.5 (https://choishingwan.github.io/PRSice/; ***Choi and O'Reilly, 2019***) was used to calculate

the PRS. PLINK 2.0 (https://www.cog-genomics.org/plink/2.0/) and FUMA version 1.5.6 (https://fuma.ctglab.nl/) were used to perform genome-wide association analysis, and ANNOVAR was used to perform gene-based annotation. AHBA microarray expression data were processed using abagen toolbox version 0.1.3 (https://doi.org/10.5281/zenodo.5129257). The rotate_parcellation code used to perform a spatial permutation test of a parcellated cortical map: https://github.com/frantisekvasa/rotate_parcellation (***Váša, 2023***; ***Váša et al., 2018***). Code for PLS analysis and bootstrapping to estimate PLS weights are available at https://github.com/KirstieJane/NSPN_WhitakerVertes_PNAS2016/tree/master/SCRIPTS (***Whitaker, 2016***; ***Whitaker et al., 2016***). clusterProfiler 4.6 in R version 4.2.0 was used to analyze gene-set enrichment.

Acknowledgements

This research used the UK Biobank Resource under application number 19542. We thank all participants and researchers from the UK Biobank. We thank the IMAGEN Consortium for providing the discover data. This work received support from the following sources: the National Nature Science Foundation of China (No.82304241 [to XL]), National Key R&D Program of China (No.2019YFA0709502 [to JF], No.2018YFC1312904 [to JF]), Shanghai Municipal Science and Technology Major Project (No.2018SHZDZX01 [to JF], ZJ Lab [to JF], and Shanghai Center for Brain Science and Brain-Inspired Technology [to JF]), the 111 Project (No.B18015 [to JF]), the European Union-funded FP6 Integrated Project IMAGEN (Reinforcement-related behaviour in normal brain function and psychopathology) (LSHM-CT- 2007–037286 [to GS]), the Horizon 2020 funded ERC Advanced Grant 'STRATIFY' (Brain network based stratification of reinforcement-related disorders) (695313 [to GS]), Human Brain Project (HBP SGA 2, 785907, and HBP SGA 3, 945539 [to GS]), the Medical Research Council Grant 'c-VEDA' (Consortium on Vulnerability to Externalizing Disorders and Addictions) (MR/N000390/1 [to GS]), the National Institute of Health (NIH) (R01DA049238 [to GS], A decentralized macro and micro gene-by-environment interaction analysis of substance use behavior and its brain biomarkers), the National Institute for Health Research (NIHR) Biomedical Research Centre at South London and Maudsley NHS Foundation Trust and King's College London, the Bundesministeriumfür Bildung und Forschung (BMBF grants 01GS08152; 01EV0711 [to GS]; Forschungsnetz AERIAL 01EE1406A, 01EE1406B; Forschungsnetz IMAC-Mind 01GL1745B [to GS]), the Deutsche Forschungsgemeinschaft (DFG grants SM 80/7–2, SFB 940, TRR 265, NE 1383/14–1 [to GS]), the Medical Research Foundation and Medical Research Council (grants MR/R00465X/1 and MR/S020306/1 [to SD]), the National Institutes of Health (NIH) funded ENIGMA (grants 5U54EB020403-05 and 1R56AG058854-01 [to SD]), NSFC grant 82150710554 [to GS] and European Union funded project 'environMENTAL', grant no: 101057429 [to GS]. Further support was provided by grants from: - the ANR (ANR-12-SAMA-0004, AAPG2019 - GeBra [to JLM]), the Eranet Neuron (AF12-NEUR0008-01 - WM2NA; and ANR-18-NEUR00002-01 - ADORe [to JLM]), the Fondation de France (00081242 [to J.-L.M.]), the Fondation pour la Recherche Médicale (DPA20140629802 [to JLM]), the Mission Interministérielle de Lutte-contre-les-Drogues-et-les-Conduites-Addictives (MILDECA [to JLM]), the Assistance-Publique-Hôpitaux-de-Paris and INSERM (interface grant [to MLPM]), Paris Sud University IDEX 2012 [to J.-LM], the Fondation de l'Avenir (grant AP-RM-17–013 [to MLPM]), the Fédération pour la Recherche sur le Cerveau [to GS]; the National Institutes of Health, Science Foundation Ireland (16/ERCD/3797 [to RW]) and by NIH Consortium grant U54 EB020403 [to SD], supported by a cross-NIH alliance that funds Big Data to Knowledge Centres of Excellence. The funders had no role in study design, data collection and analysis, decision to publish or preparation of the manuscript.

Additional information

Competing interests

Tobias Banaschewski: Dr Banaschewski served in an advisory or consultancy role for eye level, Infectopharm, Lundbeck, Medice, Neurim Pharmaceuticals, Oberberg GmbH, Roche, and Takeda. He received conference support or speaker's fee by Janssen, Medice and Takeda. He received royalities from Hogrefe, Kohlhammer, CIP Medien, Oxford University Press; the presentwork is unrelated to these relationships. Christian Büchel: Reviewing editor, *eLife*. Luise Poustka: Dr Poustka served in

an advisory or consultancy role for Roche and Viforpharm and received speaker's fee by Shire. She received royalties from Hogrefe, Kohlhammer and Schattauer. The present work is unrelated to the above grants and relationships. The other authors declare that no competing interests exist.

Funding

Funder	Grant reference number	Author
National Natural Science Foundation of China	No.82304241	Xiaolei Lin
National Key Research and Development Program of China	No.2019YFA0709502	Jianfeng Feng
National Key Research and Development Program of China	No.2018YFC1312904	Jianfeng Feng
Shanghai Municipal Science and Technology Major Project	No.2018SHZDZX01	Jianfeng Feng
ZJ Lab		Jianfeng Feng
Shanghai Center for Brain Science and Brain-Inspired Technology		Jianfeng Feng
111 project	No.B18015	Jianfeng Feng
European Union FP6 Integrated Project IMAGEN	LSHM-CT- 2007-037286	Gunter Schumann
Horizon 2020 ERC Advanced Grant 'STRATIFY'	695313	Gunter Schumann
Human Brain Project	HBP SGA 2,785907	Gunter Schumann
Human Brain Project	HBP SGA 3,945539	Gunter Schumann
Medical Research Council Grant 'c-VEDA'	MR/N000390/1	Gunter Schumann
National Institutes of Health	R01DA049238	Gunter Schumann
National Institute for Health Research (NIHR) Biomedical Research Centre at South London and Maudsley NHS Foundation Trust and King's College London		Gunter Schumann
Deutsche Forschungsgemeinschaft	SM 80/7-2	Gunter Schumann
Medical Research Foundation and Medical Research Council	MR/R00465X/1	Sylvane Desrivières
National Institutes of Health	ENIGMA 5U54EB020403-05	Sylvane Desrivières
National Institutes of Health	U54 EB020403	Sylvane Desrivières
ANR	ANR-12-SAMA-0004 AAPG2019 - GeBra	Jean-Luc Martinot
Eranet Neuron	AF12-NEUR0008-01 - WM2NA	Jean-Luc Martinot
Fondation de France	00081242	Jean-Luc Martinot

Funder	Grant reference number	Author
Fondation pour la Recherche Médicale	DPA20140629802	Jean-Luc Martinot
Mission Interministérielle de Lutte-contre-les-Drogues-et-les-Conduites-Addictives	MILDECA	Jean-Luc Martinot
Assistance-Publique-Hôpitaux-de-Paris and INSERM	interface grant	Marie-Laure Paillère Martinot
Paris Sud University IDEX 2012		Jean-Luc Martinot
Fondation de l'Avenir	AP-RM-17-013	Marie-Laure Paillère Martinot
Fédération pour la Recherche sur le Cerveau		Gunter Schumann
National Institutes of Health, Science Foundation Ireland	16/ERCD/3797	Robert Whelan
NSFC	82150710554	Gunter Schumann
environMENTAL	grant no: 101057429	Gunter Schumann
Bundesministeriumfür Bildung und Forschung	01GS08152	Gunter Schumann
Bundesministeriumfür Bildung und Forschung	01EV0711	Gunter Schumann
Forschungsnetz AERIAL	01EE1406A	Gunter Schumann
Forschungsnetz AERIAL	01EE1406B	Gunter Schumann
Forschungsnetz IMAC-Mind	01GL1745B	Gunter Schumann
Deutsche Forschungsgemeinschaft	SFB 940	Gunter Schumann
Deutsche Forschungsgemeinschaft	TRR 265	Gunter Schumann
Deutsche Forschungsgemeinschaft	NE 1383/14-1	Gunter Schumann
Medical Research Foundation and Medical Research Council	MR/S020306/1	Sylvane Desrivières
National Institutes of Health	ENIGMA 1R56AG058854-01	Sylvane Desrivières
Eranet	ANR-18-NEUR00002-01 - ADORe	Jean-Luc Martinot

The funders had no role in study design, data collection and interpretation, or the decision to submit the work for publication.

Author contributions

Haojing Duan, Software, Formal analysis, Visualization, Methodology, Writing - original draft, Writing – review and editing; Runye Shi, Data curation, Visualization, Writing – review and editing; Jujiao Kang, Tobias Banaschewski, Arun LW Bokde, Christian Büchel, Herta Flor, Antoine Grigis, Hugh Garavan, Penny A Gowland, Andreas Heinz, Rüdiger Brühl, Eric Artiges, Frauke Nees, Dimitri Papadopoulos Orfanos, Luise Poustka, Sarah Hohmann, Nathalie Nathalie Holz, Juliane Fröhner, Michael N Smolka, Nilakshi Vaidya, Henrik Walter, Data curation, Writing – review and editing; Sylvane Desrivières, Jean-Luc Martinot, Marie-Laure Paillère Martinot, Robert Whelan, Gunter Schumann, Data curation,

Funding acquisition, Writing – review and editing; Xiaolei Lin, Conceptualization, Funding acquisition, Methodology, Writing - original draft, Writing – review and editing; Jianfeng Feng, Conceptualization, Funding acquisition, Writing – review and editing

Author ORCIDs
Haojing Duan http://orcid.org/0009-0004-8659-9591
Christian Büchel https://orcid.org/0000-0003-1965-906X
Rüdiger Brühl https://orcid.org/0000-0003-0111-5996
Jean-Luc Martinot https://orcid.org/0000-0002-0136-0388
Dimitri Papadopoulos Orfanos https://orcid.org/0000-0002-1242-8990
Michael N Smolka https://orcid.org/0000-0001-5398-5569
Xiaolei Lin https://orcid.org/0000-0003-2463-1272
Jianfeng Feng https://orcid.org/0000-0001-5987-2258

Ethics
All participants from UK Biobank provided written informed consent, and ethical approval was granted by the North West Multi-Center Ethics committee (https://www.ukbiobank.ac.uk/learn-more-about-uk-biobank/about-us/ethics) with research ethics committee (REC) approval number 16/NW/0274. The IMAGEN study was approved by local ethics research committees of King's College London, University of Nottingham. Trinity College Dublin, University of Heidelberg, Technische Universität Dresden, Commissariat à l'Énergie Atomique et aux Énergies Alternatives, and University Medical Center at the University of Hamburg in compliance with the Declaration of Helsinki (https://doi.org/10.1001/jama.2013.281053). Informed consent was given by all participants and a parent/guardian of each participant.

Peer review material
Reviewer #1 (Public Review): https://doi.org/10.7554/eLife.94970.3.sa1
Reviewer #2 (Public Review): https://doi.org/10.7554/eLife.94970.3.sa2
Author response https://doi.org/10.7554/eLife.94970.3.sa3

Additional files

Supplementary files
- MDAR checklist

Data availability
The summary statistics of GWAS for individual deviations of total GMV is available at https://doi.org/10.5061/dryad.jh9w0vtmn. All the UK Biobank data used in the study are available at https://www.ukbiobank.ac.uk. The IMAGEN project data are available at https://imagen-project.org (***Schumann et al., 2010***). GWAS summary statistics used to calculate the PRS are available in the ***Appendix 1—table 8***. Human gene expression data are available in the Allen Human Brain Atlas dataset: https://human.brainmap.org (***Hawrylycz et al., 2012***). Source data files have been provided for ***Figures 2–5, 7 and 8***, which contain the numerical data used to generate the figures. Summary statistics of the GWAS for delayed brain development by Shi et al are available at https://delayedneurodevelopment.page.link/amTC.

The following dataset was generated:

Author(s)	Year	Dataset title	Dataset URL	Database and Identifier
Duan H, Shi R, Kang J	2024	The summary statistics of GWAS for individual deviations of total GMV	https://doi.org/10.5061/dryad.jh9w0vtmn	Dryad, 10.5061/dryad.jh9w0vtmn

The following previously published datasets were used:

Author(s)	Year	Dataset title	Dataset URL	Database and Identifier
Nalls MA, Blauwendraat C, Vallerga CL	2019	Parkinson's disease or first degree relation to individual with Parkinson's disease	https://www.ebi.ac.uk/gwas/studies/GCST009325	GWAS Catalog, GCST009325
Sullivan P	2021	adhd2019	https://doi.org/10.6084/m9.figshare.14671965	figshare, 10.6084/m9.figshare.14671965
Sullivan P	2019	asd2019	https://doi.org/10.6084/m9.figshare.14671989	figshare, 10.6084/m9.figshare.14671989
Jansen IE, Savage JE, Watanabe K	2019	Summary statistics for Genome-wide meta-analysis identifies new loci and functional pathways influencing Alzheimer's disease risk	https://vu.data.surfsara.nl/index.php/s/l7aiRr1UEgdoJfZ	Vrije Universiteit Research Drive, l7aiRr1UEgdoJfZ
Sullivan P	2023	bip2021_noUKBB	https://doi.org/10.6084/m9.figshare.22564402	figshare, 10.6084/m9.figshare.22564402
Adams MJ	2023	MDD2 (MDD2018) GWAS sumstats w/o UKBB	https://doi.org/10.6084/m9.figshare.21655784	figshare, 10.6084/m9.figshare.21655784
Sullivan P	2022	scz2022	https://doi.org/10.6084/m9.figshare.19426775	figshare, 10.6084/m9.figshare.19426775

References

Alexander-Bloch A, Giedd JN, Bullmore E. 2013. Imaging structural co-variance between human brain regions. *Nature Reviews. Neuroscience* **14**:322–336. DOI: https://doi.org/10.1038/nrn3465, PMID: 23531697

Aljondi R, Szoeke C, Steward C, Yates P, Desmond P. 2019. A decade of changes in brain volume and cognition. *Brain Imaging and Behavior* **13**:554–563. DOI: https://doi.org/10.1007/s11682-018-9887-z, PMID: 29744801

Association. 2013. World medical association declaration of helsinki: ethical principles for medical research involving human subjects. *JAMA* **310**:2191–2194. DOI: https://doi.org/10.1001/jama.2013.281053

Berg D, Borghammer P, Fereshtehnejad S-M, Heinzel S, Horsager J, Schaeffer E, Postuma RB. 2021. Prodromal Parkinson disease subtypes - key to understanding heterogeneity. *Nature Reviews. Neurology* **17**:349–361. DOI: https://doi.org/10.1038/s41582-021-00486-9, PMID: 33879872

Bogousslavsky J, Miklossy J, Deruaz JP, Assal G, Regli F. 1987. Lingual and fusiform gyri in visual processing: a clinico-pathologic study of superior altitudinal hemianopia. *Journal of Neurology, Neurosurgery & Psychiatry* **50**:607–614. DOI: https://doi.org/10.1136/jnnp.50.5.607

Bohl J, Brimer N, Lyons C, Vande Pol SB. 2007. The stardust family protein MPP7 forms a tripartite complex with LIN7 and DLG1 that regulates the stability and localization of DLG1 to cell junctions. *The Journal of Biological Chemistry* **282**:9392–9400. DOI: https://doi.org/10.1074/jbc.M610002200, PMID: 17237226

Brouwer RM, Klein M, Grasby KL, Schnack HG, Jahanshad N, Teeuw J, Thomopoulos SI, Sprooten E, Franz CE, Gogtay N, Kremen WS, Panizzon MS, Olde Loohuis LM, Whelan CD, Aghajani M, Alloza C, Alnæs D, Artiges E, Ayesa-Arriola R, Barker GJ, et al. 2022. Genetic variants associated with longitudinal changes in brain structure across the lifespan. *Nature Neuroscience* **25**:421–432. DOI: https://doi.org/10.1038/s41593-022-01042-4, PMID: 35383335

Chang CC, Chow CC, Tellier LC, Vattikuti S, Purcell SM, Lee JJ. 2015. Second-generation PLINK: rising to the challenge of larger and richer datasets. *GigaScience* **4**:7. DOI: https://doi.org/10.1186/s13742-015-0047-8, PMID: 25722852

Chételat G, Landeau B, Eustache F, Mézenge F, Viader F, de la Sayette V, Desgranges B, Baron J-C. 2005. Using voxel-based morphometry to map the structural changes associated with rapid conversion in MCI: a longitudinal MRI study. *NeuroImage* **27**:934–946. DOI: https://doi.org/10.1016/j.neuroimage.2005.05.015, PMID: 15979341

Choi SW, O'Reilly PF. 2019. PRSice-2: Polygenic Risk Score software for biobank-scale data. *GigaScience* **8**:giz082. DOI: https://doi.org/10.1093/gigascience/giz082, PMID: 31307061

Christman S, Bermudez C, Hao L, Landman BA, Boyd B, Albert K, Woodward N, Shokouhi S, Vega J, Andrews P, Taylor WD. 2020. Accelerated brain aging predicts impaired cognitive performance and greater disability in

geriatric but not midlife adult depression. *Translational Psychiatry* **10**:317. DOI: https://doi.org/10.1038/s41398-020-01004-z, PMID: 32948749

Codd V, Wang Q, Allara E, Musicha C, Kaptoge S, Stoma S, Jiang T, Hamby SE, Braund PS, Bountziouka V, Budgeon CA, Denniff M, Swinfield C, Papakonstantinou M, Sheth S, Nanus DE, Warner SC, Wang M, Khera AV, Eales J, et al. 2021. Polygenic basis and biomedical consequences of telomere length variation. *Nature Genetics* **53**:1425–1433. DOI: https://doi.org/10.1038/s41588-021-00944-6, PMID: 34611362

Courchesne E, Chisum HJ, Townsend J, Cowles A, Covington J, Egaas B, Harwood M, Hinds S, Press GA. 2000. Normal brain development and aging: quantitative analysis at in vivo MR imaging in healthy volunteers. *Radiology* **216**:672–682. DOI: https://doi.org/10.1148/radiology.216.3.r00au37672, PMID: 10966694

Demanelis K, Jasmine F, Chen LS, Chernoff M, Tong L, Delgado D, Zhang C, Shinkle J, Sabarinathan M, Lin H, Ramirez E, Oliva M, Kim-Hellmuth S, Stranger BE, Lai TP, Aviv A, Ardlie KG, Aguet F, Ahsan H, GTEx Consortium, et al. 2020. Determinants of telomere length across human tissues. *Science* **369**:eaaz6876. DOI: https://doi.org/10.1126/science.aaz6876, PMID: 32913074

Demontis D, Walters RK, Martin J, Mattheisen M, Als TD, Agerbo E, Baldursson G, Belliveau R, Bybjerg-Grauholm J, Bækvad-Hansen M, Cerrato F, Chambert K, Churchhouse C, Dumont A, Eriksson N, Gandal M, Goldstein JI, Grasby KL, Grove J, Gudmundsson OO, et al. 2019. Discovery of the first genome-wide significant risk loci for attention deficit/hyperactivity disorder. *Nature Genetics* **51**:63–75. DOI: https://doi.org/10.1038/s41588-018-0269-7, PMID: 30478444

Desikan RS, Ségonne F, Fischl B, Quinn BT, Dickerson BC, Blacker D, Buckner RL, Dale AM, Maguire RP, Hyman BT, Albert MS, Killiany RJ. 2006. An automated labeling system for subdividing the human cerebral cortex on MRI scans into gyral based regions of interest. *NeuroImage* **31**:968–980. DOI: https://doi.org/10.1016/j.neuroimage.2006.01.021, PMID: 16530430

Douaud G, Groves AR, Tamnes CK, Westlye LT, Duff EP, Engvig A, Walhovd KB, James A, Gass A, Monsch AU, Matthews PM, Fjell AM, Smith SM, Johansen-Berg H. 2014. A common brain network links development, aging, and vulnerability to disease. *PNAS* **111**:17648–17653. DOI: https://doi.org/10.1073/pnas.1410378111, PMID: 25422429

Elliott ML, Belsky DW, Knodt AR, Ireland D, Melzer TR, Poulton R, Ramrakha S, Caspi A, Moffitt TE, Hariri AR. 2021. Brain-age in midlife is associated with accelerated biological aging and cognitive decline in a longitudinal birth cohort. *Molecular Psychiatry* **26**:3829–3838. DOI: https://doi.org/10.1038/s41380-019-0626-7, PMID: 31822815

Epstein R, Harris A, Stanley D, Kanwisher N. 1999. The parahippocampal place area: recognition, navigation, or encoding? *Neuron* **23**:115–125. DOI: https://doi.org/10.1016/s0896-6273(00)80758-8, PMID: 10402198

Estrada K, Styrkarsdottir U, Evangelou E, Hsu Y-H, Duncan EL, Ntzani EE, Oei L, Albagha OME, Amin N, Kemp JP, Koller DL, Li G, Liu C-T, Minster RL, Moayyeri A, Vandenput L, Willner D, Xiao S-M, Yerges-Armstrong LM, Zheng H-F, et al. 2012. Genome-wide meta-analysis identifies 56 bone mineral density loci and reveals 14 loci associated with risk of fracture. *Nature Genetics* **44**:491–501. DOI: https://doi.org/10.1038/ng.2249, PMID: 22504420

Feczko E, Miranda-Dominguez O, Marr M, Graham AM, Nigg JT, Fair DA. 2019. The heterogeneity problem: approaches to identify psychiatric subtypes. *Trends in Cognitive Sciences* **23**:584–601. DOI: https://doi.org/10.1016/j.tics.2019.03.009

Ferreira D, Nordberg A, Westman E. 2020. Biological subtypes of Alzheimer disease: a systematic review and meta-analysis. *Neurology* **94**:436–448. DOI: https://doi.org/10.1212/WNL.0000000000009058, PMID: 32047067

Fischl B, Salat DH, Busa E, Albert M, Dieterich M, Haselgrove C, van der Kouwe A, Killiany R, Kennedy D, Klaveness S, Montillo A, Makris N, Rosen B, Dale AM. 2002. Whole brain segmentation: automated labeling of neuroanatomical structures in the human brain. *Neuron* **33**:341–355. DOI: https://doi.org/10.1016/s0896-6273(02)00569-x, PMID: 11832223

Fjell AM, Walhovd KB. 2010. Structural brain changes in aging: courses, causes and cognitive consequences. *Reviews in the Neurosciences* **21**:187–221. DOI: https://doi.org/10.1515/revneuro.2010.21.3.187, PMID: 20879692

Fjell AM, Grydeland H, Krogsrud SK, Amlien I, Rohani DA, Ferschmann L, Storsve AB, Tamnes CK, Sala-Llonch R, Due-Tønnessen P, Bjørnerud A, Sølsnes AE, Håberg AK, Skranes J, Bartsch H, Chen CH, Thompson WK, Panizzon MS, Kremen WS, Dale AM, et al. 2015. Development and aging of cortical thickness correspond to genetic organization patterns. *PNAS* **112**:15462–15467. DOI: https://doi.org/10.1073/pnas.1508831112, PMID: 26575625

Foster HME, Celis-Morales CA, Nicholl BI, Petermann-Rocha F, Pell JP, Gill JMR, O'Donnell CA, Mair FS. 2018. The effect of socioeconomic deprivation on the association between an extended measurement of unhealthy lifestyle factors and health outcomes: a prospective analysis of the UK Biobank cohort. *The Lancet. Public Health* **3**:e576–e585. DOI: https://doi.org/10.1016/S2468-2667(18)30200-7, PMID: 30467019

Ghafouri-Fard S, Khoshbakht T, Taheri M, Ghanbari M. 2021. A concise review on the role of BDNF-AS in human disorders. *Biomedicine & Pharmacotherapy* **142**:112051. DOI: https://doi.org/10.1016/j.biopha.2021.112051

Glahn DC, Kent JW, Sprooten E, Diego VP, Winkler AM, Curran JE, McKay DR, Knowles EE, Carless MA, Göring HHH, Dyer TD, Olvera RL, Fox PT, Almasy L, Charlesworth J, Kochunov P, Duggirala R, Blangero J. 2013. Genetic basis of neurocognitive decline and reduced white-matter integrity in normal human brain aging. *PNAS* **110**:19006–19011. DOI: https://doi.org/10.1073/pnas.1313735110, PMID: 24191011

Grønborg M, Kristiansen TZ, Iwahori A, Chang R, Reddy R, Sato N, Molina H, Jensen ON, Hruban RH, Goggins MG, Maitra A, Pandey A. 2006. Biomarker discovery from pancreatic cancer secretome using a

differential proteomic approach. *Molecular & Cellular Proteomics* **5**:157–171. DOI: https://doi.org/10.1074/mcp.M500178-MCP200

Grove J, Ripke S, Als TD, Mattheisen M, Walters RK, Won H, Pallesen J, Agerbo E, Andreassen OA, Anney R, Awashti S, Belliveau R, Bettella F, Buxbaum JD, Bybjerg-Grauholm J, Bækvad-Hansen M, Cerrato F, Chambert K, Christensen JH, Churchhouse C, et al. 2019. Identification of common genetic risk variants for autism spectrum disorder. *Nature Genetics* **51**:431–444. DOI: https://doi.org/10.1038/s41588-019-0344-8, PMID: 30804558

Habes M, Grothe MJ, Tunc B, McMillan C, Wolk DA, Davatzikos C. 2020. Disentangling heterogeneity in Alzheimer's disease and related dementias using data-driven methods. *Biological Psychiatry* **88**:70–82. DOI: https://doi.org/10.1016/j.biopsych.2020.01.016, PMID: 32201044

Hawrylycz MJ, Lein ES, Guillozet-Bongaarts AL, Shen EH, Ng L, Miller JA, van de Lagemaat LN, Smith KA, Ebbert A, Riley ZL, Abajian C, Beckmann CF, Bernard A, Bertagnolli D, Boe AF, Cartagena PM, Chakravarty MM, Chapin M, Chong J, Dalley RA, et al. 2012. An anatomically comprehensive atlas of the adult human brain transcriptome. *Nature* **489**:391–399. DOI: https://doi.org/10.1038/nature11405, PMID: 22996553

Honea R, Crow TJ, Passingham D, Mackay CE. 2005. Regional deficits in brain volume in schizophrenia: a meta-analysis of voxel-based morphometry studies. *The American Journal of Psychiatry* **162**:2233–2245. DOI: https://doi.org/10.1176/appi.ajp.162.12.2233, PMID: 16330585

Hoogman M, Muetzel R, Guimaraes JP, Shumskaya E, Mennes M, Zwiers MP, Jahanshad N, Sudre G, Wolfers T, Earl EA, Soliva Vila JC, Vives-Gilabert Y, Khadka S, Novotny SE, Hartman CA, Heslenfeld DJ, Schweren LJS, Ambrosino S, Oranje B, de Zeeuw P, et al. 2019. Brain imaging of the cortex in adhd: a coordinated analysis of large-scale clinical and population-based samples. *The American Journal of Psychiatry* **176**:531–542. DOI: https://doi.org/10.1176/appi.ajp.2019.18091033, PMID: 31014101

Imagen. 2020. Imagen_mri. 7548010. GitHub. https://github.com/imagen2/imagen_mri

Jansen IE, Savage JE, Watanabe K, Bryois J, Williams DM, Steinberg S, Sealock J, Karlsson IK, Hägg S, Athanasiu L, Voyle N, Proitsi P, Witoelar A, Stringer S, Aarsland D, Almdahl IS, Andersen F, Bergh S, Bettella F, Bjornsson S, et al. 2019. Genome-wide meta-analysis identifies new loci and functional pathways influencing Alzheimer's disease risk. *Nature Genetics* **51**:404–413. DOI: https://doi.org/10.1038/s41588-018-0311-9, PMID: 30617256

Kaech SM, Whitfield CW, Kim SK. 1998. The LIN-2/LIN-7/LIN-10 complex mediates basolateral membrane localization of the *C. elegans* EGF receptor LET-23 in vulval epithelial cells. *Cell* **94**:761–771. DOI: https://doi.org/10.1016/s0092-8674(00)81735-3, PMID: 9753323

Kaufmann T, van der Meer D, Doan NT, Schwarz E, Lund MJ, Agartz I, Alnæs D, Barch DM, Baur-Streubel R, Bertolino A, Bettella F, Beyer MK, Bøen E, Borgwardt S, Brandt CL, Buitelaar J, Celius EG, Cervenka S, Conzelmann A, Córdova-Palomera A, et al. 2019. Common brain disorders are associated with heritable patterns of apparent aging of the brain. *Nature Neuroscience* **22**:1617–1623. DOI: https://doi.org/10.1038/s41593-019-0471-7, PMID: 31551603

Lanktree M, Squassina A, Krinsky M, Strauss J, Jain U, Macciardi F, Kennedy JL, Muglia P. 2008. Association study of brain-derived neurotrophic factor (BDNF) and LIN-7 homolog (LIN-7) genes with adult attention-deficit/hyperactivity disorder. *American Journal of Medical Genetics. Part B, Neuropsychiatric Genetics* **147B**:945–951. DOI: https://doi.org/10.1002/ajmg.b.30723, PMID: 18286632

Levine ME, Lu AT, Quach A, Chen BH, Assimes TL, Bandinelli S, Hou L, Baccarelli AA, Stewart JD, Li Y, Whitsel EA, Wilson JG, Reiner AP, Aviv A, Lohman K, Liu Y, Ferrucci L, Horvath S. 2018. An epigenetic biomarker of aging for lifespan and healthspan. *Aging* **10**:573–591. DOI: https://doi.org/10.18632/aging.101414, PMID: 29676998

Li J, Seidlitz J, Suckling J, Fan F, Ji G-J, Meng Y, Yang S, Wang K, Qiu J, Chen H, Liao W. 2021. Cortical structural differences in major depressive disorder correlate with cell type-specific transcriptional signatures. *Nature Communications* **12**:1647. DOI: https://doi.org/10.1038/s41467-021-21943-5

Liu L, Watanabe N, Akatsu H, Nishimura M. 2016. Neuronal expression of ILEI/FAM3C and its reduction in Alzheimer's disease. *Neuroscience* **330**:236–246. DOI: https://doi.org/10.1016/j.neuroscience.2016.05.050, PMID: 27256505

Mariani E, Polidori MC, Cherubini A, Mecocci P. 2005. Oxidative stress in brain aging, neurodegenerative and vascular diseases: An overview. *Journal of Chromatography B* **827**:65–75. DOI: https://doi.org/10.1016/j.jchromb.2005.04.023

Markello RD, Arnatkeviciute A, Poline J-B, Fulcher BD, Fornito A, Misic B. 2021. Standardizing workflows in imaging transcriptomics with the abagen toolbox. *eLife* **10**:e72129. DOI: https://doi.org/10.7554/eLife.72129, PMID: 34783653

Mattson MP, Arumugam TV. 2018. Hallmarks of brain aging: adaptive and pathological modification by metabolic states. *Cell Metabolism* **27**:1176–1199. DOI: https://doi.org/10.1016/j.cmet.2018.05.011, PMID: 29874566

McGinnis SM, Brickhouse M, Pascual B, Dickerson BC. 2011. Age-related changes in the thickness of cortical zones in humans. *Brain Topography* **24**:279–291. DOI: https://doi.org/10.1007/s10548-011-0198-6, PMID: 21842406

Mechelli A, Humphreys GW, Mayall K, Olson A, Price CJ. 2000. Differential effects of word length and visual contrast in the fusiform and lingual gyri during. *Proceedings of the Royal Society of London. Series B* **267**:1909–1913. DOI: https://doi.org/10.1098/rspb.2000.1229

Morgan SE, Seidlitz J, Whitaker KJ, Romero-Garcia R, Clifton NE, Scarpazza C, van Amelsvoort T, Marcelis M, van Os J, Donohoe G, Mothersill D, Corvin A, Pocklington A, Raznahan A, McGuire P, Vértes PE, Bullmore ET.

2019. Cortical patterning of abnormal morphometric similarity in psychosis is associated with brain expression of schizophrenia-related genes. *PNAS* **116**:9604–9609. DOI: https://doi.org/10.1073/pnas.1820754116

Mullins N, Forstner AJ, O'Connell KS, Coombes B, Coleman JRI, Qiao Z, Als TD, Bigdeli TB, Børte S, Bryois J, Charney AW, Drange OK, Gandal MJ, Hagenaars SP, Ikeda M, Kamitaki N, Kim M, Krebs K, Panagiotaropoulou G, Schilder BM, et al. 2021. Genome-wide association study of more than 40,000 bipolar disorder cases provides new insights into the underlying biology. *Nature Genetics* **53**:817–829. DOI: https://doi.org/10.1038/s41588-021-00857-4, PMID: 34002096

Nalls MA, Blauwendraat C, Vallerga CL, Heilbron K, Bandres-Ciga S, Chang D, Tan M, Kia DA, Noyce AJ, Xue A, Bras J, Young E, von Coelln R, Simón-Sánchez J, Schulte C, Sharma M, Krohn L, Pihlstrøm L, Siitonen A, Iwaki H, et al. 2019. Identification of novel risk loci, causal insights, and heritable risk for Parkinson's disease: a meta-analysis of genome-wide association studies. *The Lancet. Neurology* **18**:1091–1102. DOI: https://doi.org/10.1016/S1474-4422(19)30320-5, PMID: 31701892

Nyberg L, Andersson M, Lundquist A, Baaré WFC, Bartrés-Faz D, Bertram L, Boraxbekk CJ, Brandmaier AM, Demnitz N, Drevon CA, Duezel S, Ebmeier KP, Ghisletta P, Henson R, Jensen DEA, Kievit RA, Knights E, Kühn S, Lindenberger U, Plachti A, et al. 2023. Individual differences in brain aging: heterogeneity in cortico-hippocampal but not caudate atrophy rates. *Cerebral Cortex* **33**:5075–5081. DOI: https://doi.org/10.1093/cercor/bhac400, PMID: 36197324

Park DC, Reuter-Lorenz P. 2009. The adaptive brain: aging and neurocognitive scaffolding. *Annual Review of Psychology* **60**:173–196. DOI: https://doi.org/10.1146/annurev.psych.59.103006.093656, PMID: 19035823

Poulakis K, Pereira JB, Muehlboeck J-S, Wahlund L-O, Smedby Ö, Volpe G, Masters CL, Ames D, Niimi Y, Iwatsubo T, Ferreira D, Westman E, Japanese Alzheimer's Disease Neuroimaging Initiative, Australian Imaging, Biomarkers and Lifestyle study. 2022. Multi-cohort and longitudinal Bayesian clustering study of stage and subtype in Alzheimer's disease. *Nature Communications* **13**:4566. DOI: https://doi.org/10.1038/s41467-022-32202-6, PMID: 35931678

Raz N. 2000. *Aging of the brain and its impact on cognitive performance: integration of structural and functional findings*. University of Memphis.

Raz N, Rodrigue KM. 2006. Differential aging of the brain: patterns, cognitive correlates and modifiers. *Neuroscience & Biobehavioral Reviews* **30**:730–748. DOI: https://doi.org/10.1016/j.neubiorev.2006.07.001

Raz N, Ghisletta P, Rodrigue KM, Kennedy KM, Lindenberger U. 2010. Trajectories of brain aging in middle-aged and older adults: regional and individual differences. *NeuroImage* **51**:501–511. DOI: https://doi.org/10.1016/j.neuroimage.2010.03.020, PMID: 20298790

Romero-Garcia R, Seidlitz J, Whitaker KJ, Morgan SE, Fonagy P, Dolan RJ, Jones PB, Goodyer IM, Suckling J, NSPN Consortium, Vértes PE, Bullmore ET. 2020. Schizotypy-related magnetization of cortex in healthy adolescence is colocated with expression of schizophrenia-related genes. *Biological Psychiatry* **88**:248–259. DOI: https://doi.org/10.1016/j.biopsych.2019.12.005, PMID: 32029217

Roweis ST, Saul LK. 2000. Nonlinear dimensionality reduction by locally linear embedding. *Science* **290**:2323–2326. DOI: https://doi.org/10.1126/science.290.5500.2323, PMID: 11125150

Schultz CC, Koch K, Wagner G, Roebel M, Nenadic I, Gaser C, Schachtzabel C, Reichenbach JR, Sauer H, Schlösser RGM. 2010. Increased parahippocampal and lingual gyrification in first-episode schizophrenia. *Schizophrenia Research* **123**:137–144. DOI: https://doi.org/10.1016/j.schres.2010.08.033, PMID: 20850277

Schumann G, Loth E, Banaschewski T, Barbot A, Barker G, Büchel C, Conrod PJ, Dalley JW, Flor H, Gallinat J, Garavan H, Heinz A, Itterman B, Lathrop M, Mallik C, Mann K, Martinot JL, Paus T, Poline JB, Robbins TW, et al. 2010. The IMAGEN study: reinforcement-related behaviour in normal brain function and psychopathology. *Molecular Psychiatry* **15**:1128–1139. DOI: https://doi.org/10.1038/mp.2010.4, PMID: 21102431

Shaw P, Kabani NJ, Lerch JP, Eckstrand K, Lenroot R, Gogtay N, Greenstein D, Clasen L, Evans A, Rapoport JL, Giedd JN, Wise SP. 2008. Neurodevelopmental trajectories of the human cerebral cortex. *The Journal of Neuroscience* **28**:3586–3594. DOI: https://doi.org/10.1523/JNEUROSCI.5309-07.2008, PMID: 18385317

Shi R, Xiang S, Jia T, Robbins TW, Kang J, Banaschewski T, Barker GJ, Bokde ALW, Desrivières S, Flor H, Grigis A, Garavan H, Gowland P, Heinz A, Brühl R, Martinot JL, Martinot MLP, Artiges E, Nees F, Orfanos DP, et al. 2023. Structural Neurodevelopment at the Individual Level - a Life-Course Investigation Using ABCD, IMAGEN and UK Biobank Data. *medRxiv*. DOI: https://doi.org/10.1101/2023.09.20.23295841, PMID: 37790416

Smith SM, Elliott LT, Alfaro-Almagro F, McCarthy P, Nichols TE, Douaud G, Miller KL. 2020. Brain aging comprises many modes of structural and functional change with distinct genetic and biophysical associations. *eLife* **9**:e52677. DOI: https://doi.org/10.7554/eLife.52677, PMID: 32134384

Smith SM, Douaud G, Chen W, Hanayik T, Alfaro-Almagro F, Sharp K, Elliott LT. 2021. An expanded set of genome-wide association studies of brain imaging phenotypes in UK Biobank. *Nature Neuroscience* **24**:737–745. DOI: https://doi.org/10.1038/s41593-021-00826-4, PMID: 33875891

Suzuki H, Venkataraman AV, Bai W, Guitton F, Guo Y, Dehghan A, Matthews PM, Alzheimer's Disease Neuroimaging Initiative. 2019. Associations of regional brain structural differences with aging, modifiable risk factors for dementia, and cognitive performance. *JAMA Network Open* **2**:e1917257. DOI: https://doi.org/10.1001/jamanetworkopen.2019.17257, PMID: 31825506

Tamnes CK, Walhovd KB, Dale AM, Østby Y, Grydeland H, Richardson G, Westlye LT, Roddey JC, Hagler DJ, Due-Tønnessen P, Holland D, Fjell AMAlzheimer's Disease Neuroimaging Initiative2013. Brain development and aging: overlapping and unique patterns of change. *NeuroImage* **68**:63–74. DOI: https://doi.org/10.1016/j.neuroimage.2012.11.039, PMID: 23246860

Thompson DJ, Wells D, Selzam S, Peneva I, Moore R, Sharp K, Tarran WA, Beard EJ, Riveros-Mckay F, Giner-Delgado C, Palmer D, Seth P, Harrison J, Futema M, McVean G, Plagnol V, Donnelly P, Weale ME, Genomics England Research Consortium. 2022. UK Biobank release and systematic evaluation of optimised polygenic risk scores for 53 diseases and quantitative traits. *medRxiv*. DOI: https://doi.org/10.1101/2022.06.16.22276246

Tian YE, Cropley V, Maier AB, Lautenschlager NT, Breakspear M, Zalesky A. 2023. Heterogeneous aging across multiple organ systems and prediction of chronic disease and mortality. *Nature Medicine* **29**:1221–1231. DOI: https://doi.org/10.1038/s41591-023-02296-6, PMID: 37024597

Townsend P, Phillimore P, Beattie A. 2023. *Health and deprivation: inequality and the north*. Taylor & Francis.

Trubetskoy V, Pardiñas AF, Qi T, Panagiotaropoulou G, Awasthi S, Bigdeli TB, Bryois J, Chen C-Y, Dennison CA, Hall LS, Lam M, Watanabe K, Frei O, Ge T, Harwood JC, Koopmans F, Magnusson S, Richards AL, Sidorenko J, Wu Y, et al. 2022. Mapping genomic loci implicates genes and synaptic biology in schizophrenia. *Nature* **604**:502–508. DOI: https://doi.org/10.1038/s41586-022-04434-5, PMID: 35396580

Váša F, Seidlitz J, Romero-Garcia R, Whitaker KJ, Rosenthal G, Vértes PE, Shinn M, Alexander-Bloch A, Fonagy P, Dolan RJ, Jones PB, Goodyer IM, NSPN consortium, Sporns O, Bullmore ET. 2018. Adolescent tuning of association cortex in human structural brain networks. *Cerebral Cortex* **28**:281–294. DOI: https://doi.org/10.1093/cercor/bhx249, PMID: 29088339

Váša F. 2023. Rotate_parcellation. 65673ea. GitHub. https://github.com/frantisekvasa/rotate_parcellation

Wang K, Li M, Hakonarson H. 2010. ANNOVAR: functional annotation of genetic variants from high-throughput sequencing data. *Nucleic Acids Research* **38**:e164– . DOI: https://doi.org/10.1093/nar/gkq603, PMID: 20601685

Watanabe K, Taskesen E, van Bochoven A, Posthuma D. 2017. Functional mapping and annotation of genetic associations with FUMA. *Nature Communications* **8**:1826. DOI: https://doi.org/10.1038/s41467-017-01261-5, PMID: 29184056

Whitaker K. 2016. NSPN_WhitakerVertes_PNAS2016. 6950a4d. GitHub. https://github.com/KirstieJane/NSPN_WhitakerVertes_PNAS2016/tree/master/SCRIPTS

Whitaker KJ, Vértes PE, Romero-Garcia R, Váša F, Moutoussis M, Prabhu G, Weiskopf N, Callaghan MF, Wagstyl K, Rittman T, Tait R, Ooi C, Suckling J, Inkster B, Fonagy P, Dolan RJ, Jones PB, Goodyer IM, Bullmore ET, NSPN Consortium. 2016. Adolescence is associated with genomically patterned consolidation of the hubs of the human brain connectome. *PNAS* **113**:9105–9110. DOI: https://doi.org/10.1073/pnas.1601745113, PMID: 27457931

Whitwell JL, Przybelski SA, Weigand SD, Ivnik RJ, Vemuri P, Gunter JL, Senjem ML, Shiung MM, Boeve BF, Knopman DS, Parisi JE, Dickson DW, Petersen RC, Jack CR Jr, Josephs KA. 2009. Distinct anatomical subtypes of the behavioural variant of frontotemporal dementia: a cluster analysis study. *Brain* **132**:2932–2946. DOI: https://doi.org/10.1093/brain/awp232, PMID: 19762452

Wray NR, Ripke S, Mattheisen M, Trzaskowski M, Byrne EM, Abdellaoui A, Adams MJ, Agerbo E, Air TM, Andlauer TMF, Bacanu SA, Bækvad-Hansen M, Beekman AFT, Bigdeli TB, Binder EB, Blackwood DRH, Bryois J, Buttenschøn HN, Bybjerg-Grauholm J, Cai N, et al. 2018. Genome-wide association analyses identify 44 risk variam genomics of parkinson's disease consortiumnts and refine the genetic architecture of major depression. *Nature Genetics* **50**:668–681. DOI: https://doi.org/10.1038/s41588-018-0090-3, PMID: 29700475

Yao Z, Zhang Y, Lin L, Zhou Y, Xu C, Jiang T. 2010. Abnormal cortical networks in mild cognitive impairment and Alzheimer's disease. *PLOS Computational Biology* **6**:e1001006. DOI: https://doi.org/10.1371/journal.pcbi.1001006, PMID: 21124954

Yu G, Wang LG, Han Y, He QY. 2012. clusterProfiler: an R package for comparing biological themes among gene clusters. *Omics* **16**:284–287. DOI: https://doi.org/10.1089/omi.2011.0118, PMID: 22455463

Zheng H-F, Forgetta V, Hsu Y-H, Estrada K, Rosello-Diez A, Leo PJ, Dahia CL, Park-Min KH, Tobias JH, Kooperberg C, Kleinman A, Styrkarsdottir U, Liu C-T, Uggla C, Evans DS, Nielson CM, Walter K, Pettersson-Kymmer U, McCarthy S, Eriksson J, et al. 2015. Whole-genome sequencing identifies EN1 as a determinant of bone density and fracture. *Nature* **526**:112–117. DOI: https://doi.org/10.1038/nature14878, PMID: 26367794

Appendix 1

Population clustering of structural brain aging and its association with brain development.

Supplementary method

Cognitive assessment

Reaction time

This cognitive function test is based on 12 rounds of the card-game 'Snap'. The participant is shown two cards at a time; if both cards are the same, they press a button-box that is on the table in front of them as quickly as possible. The score used for analysis is mean time to correctly identify matches (UK Biobank data field 20023), which is the mean duration to first press of snap-button summed over rounds in which both cards matched.

Numeric memory

The participant was shown a 2-digit number to remember. The number then disappeared and after a short while they were asked to enter the number onto the screen. The number became one digit longer each time they remembered correctly (up to a maximum of 12 digits). This test is available for a subset of participants. The score used for analysis is maximum digits remembered correctly (UK Biobank data field 4282), which is longest number correctly recalled during the numeric memory test.

Fluid intelligence / reasoning

'Fluid intelligence' is defined as the capacity to solve problems that require logic and reasoning ability, independent of acquired knowledge. The participant has 2 min to complete as many questions as possible from the test. This test was incorporated into the touchscreen towards the end of recruitment. The score used for analysis is fluid intelligence score (UK Biobank data field 20016), which is a simple unweighted sum of the number of correct answers given to the 13 fluid intelligence questions. Participants who did not answer all of the questions within the allotted 2 min limit are scored as zero for each of the unattempted questions.

Trail making

The participant was presented with sets of digits/letters in circles scattered around the screen and asked to click on them sequentially according to a specific algorithm. The scores used for analysis are duration to complete numeric path (trail #1) (UK Biobank data field 6348) and duration to complete alphanumeric path (trail #2) (UK Biobank data field 6350).

Matrix pattern completion

The participant was presented with a series of matrix pattern blocks with an element missing and asked to select the element that best completed the pattern from a range of displayed choices. The score used for analysis is number of puzzles correctly solved (UK Biobank data field 6373).

Symbol digit substitution

The participant was presented with one grid linking symbols to single-digit integers and a second grid containing only the symbols. They were then asked to indicate the numbers attached to each of the symbols in the second grid using the first one as a key. The score used for analysis is number of symbol digit matches made correctly (UK Biobank data field 23324).

Tower rearranging

The participant was presented with an illustration of three pegs (towers) on which three differently-colored hoops had been placed. The were then asked to indicate how many moves it would take to re-arrange the hoops into another specific position. The score used for analysis is number of puzzles correct (UK Biobank data field 21004).

Paired associate learning

In the paired associate learning test the participants were shown 12 pairs of words (for 30 s in total) then, after an interval (in which they did a different test), presented with the first word of 10 of these

pairs and asked to select the matching second word from a choice of four alternatives. The words were presented in the order: huge, happy, tattered, old, long, red, sulking, pretty, tiny and new. The score used for analysis is number of word pairs correctly associated (UK Biobank data field 21097), which is the number of word pairs correctly associated out of 10 attempts.

Prospective memory

Early in the touchscreen cognitive section, the participant is shown the message "At the end of the games we will show you four colored shapes and ask you to touch the Blue Square. However, to test your memory, we want you to actually touch the Orange Circle instead." The score used for analysis is prospective memory result (UK Biobank data field 20018), which condenses the results of the prospective memory test into 3 groups ("0": instruction not recalled, either skipped or incorrect, "1": correct recall on first attempt, "2": correct recall on second attempt). We divided the test results into two groups for simplicity of analysis: "0" indicating no correct recall, and the combination of "1" and "2" indicating correct recall.

Pairs matching

Participants are asked to memorize the position of as many matching pairs of cards as possible. The cards are then turned face down on the screen and the participant is asked to touch as many pairs as possible in the fewest tries. Multiple rounds were conducted. The first round used 3 pairs of cards and the second 6 pairs of cards. In the pilot phase an additional (i.e. third) round was conducted using six pairs of cards. However this was dropped from the main study as the extra set of results were very similar to the second and not felt to add significant new information. The score used for analysis is number of incorrect matches in round 2 (UK Biobank data field 399.2).

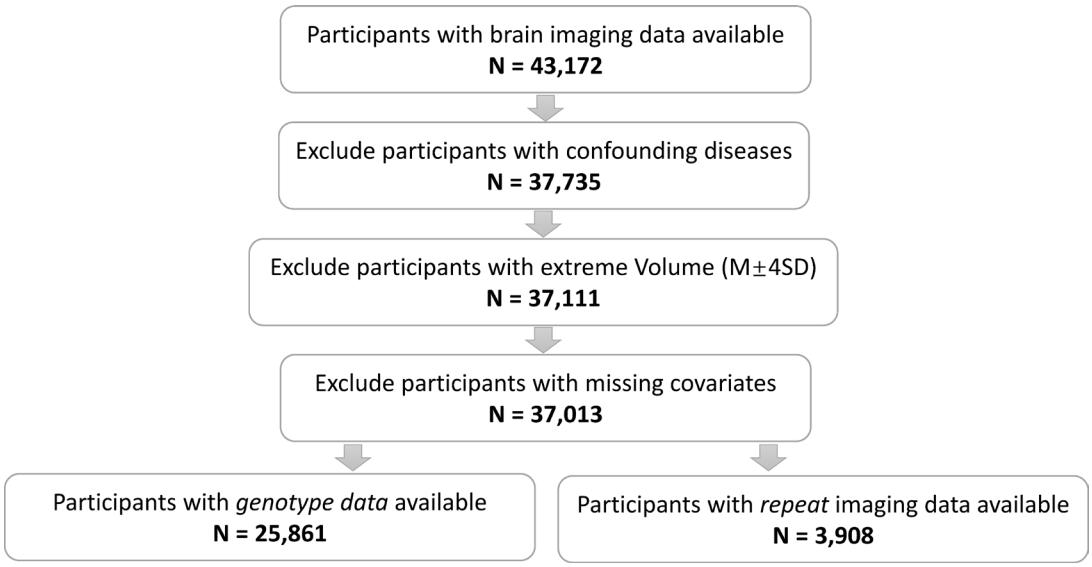

Appendix 1—figure 1. The sample selection workflow.

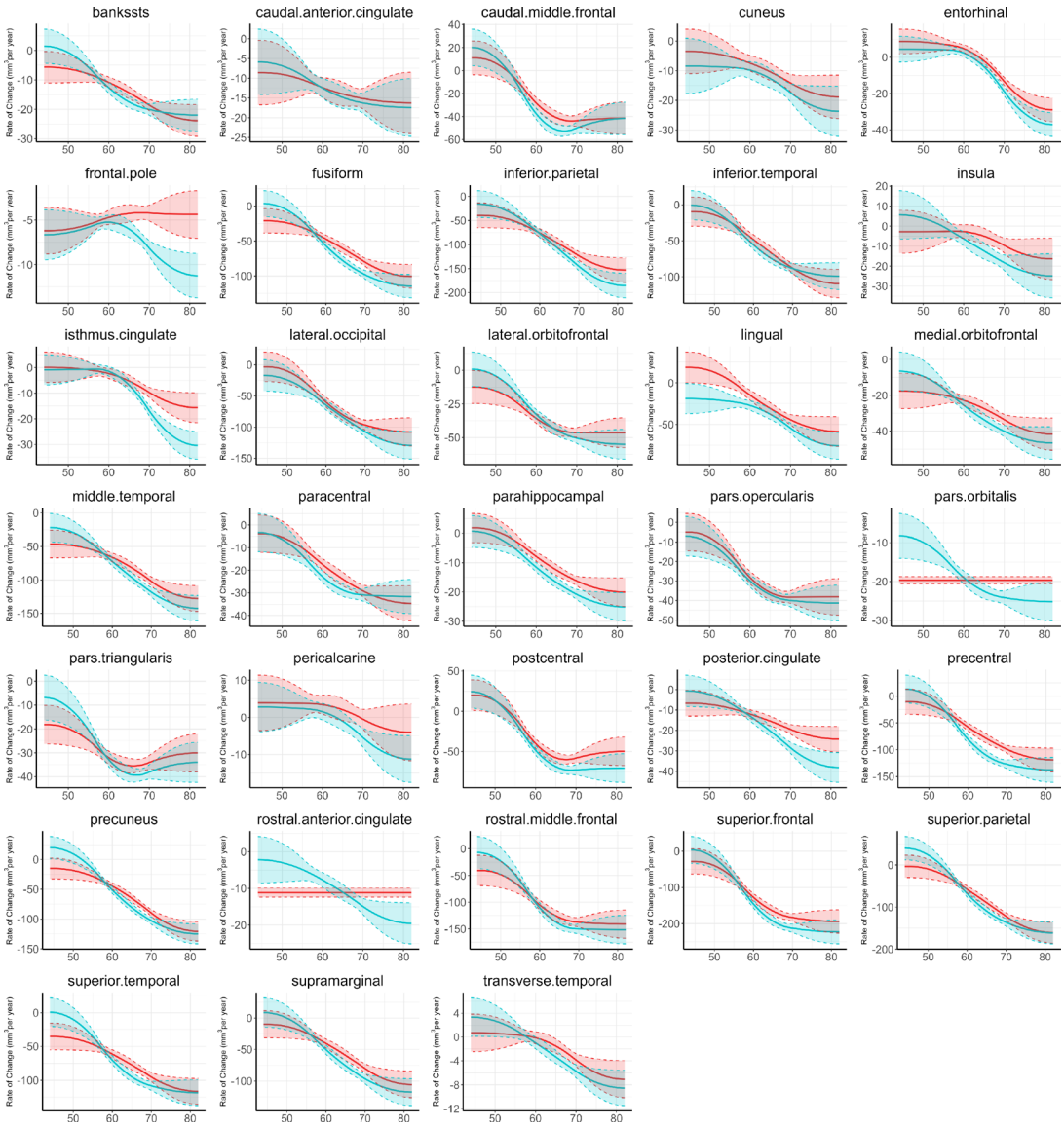

Appendix 1—figure 2. Estimated rates of change in regional volumes for 33 bilateral brain regions.

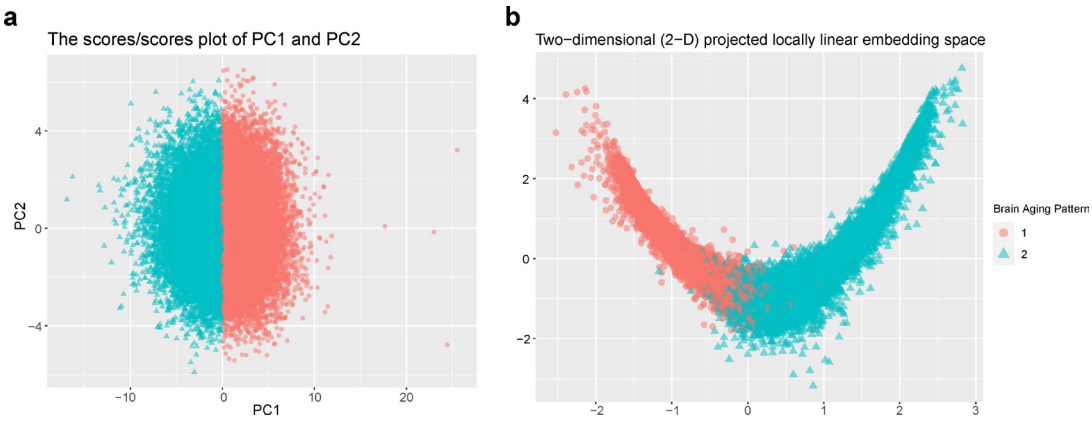

Appendix 1—figure 3. Stratification of the identified brain aging patterns using linear and non-linear dimensionality reduction methods.

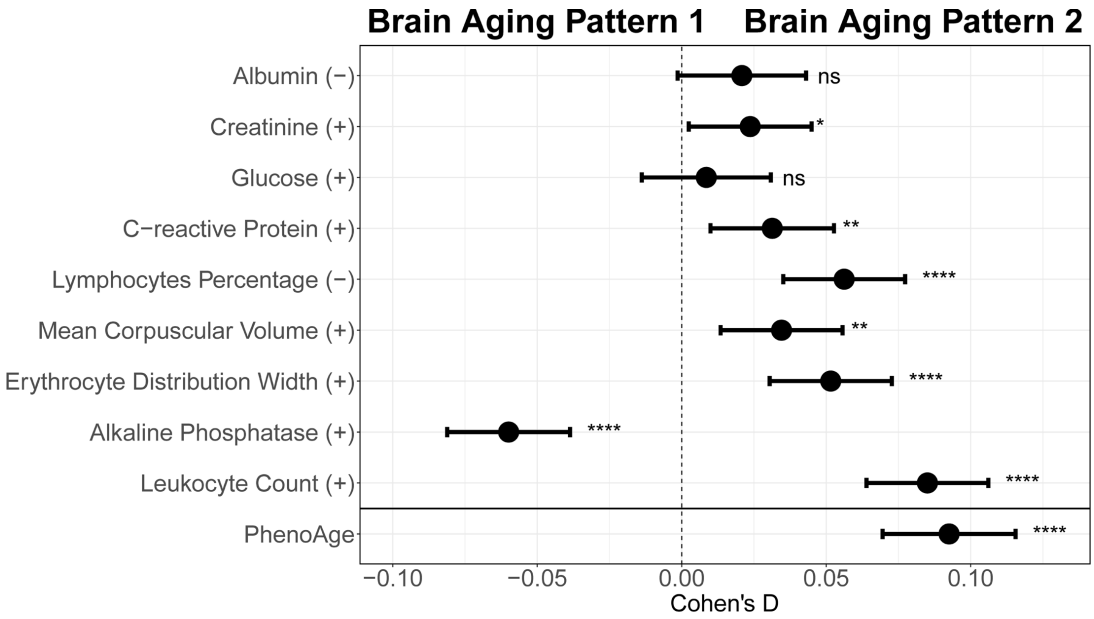

Appendix 1—figure 4. Effect size for comparing each individual blood biochemical metric (used to calculate the PhenoAge) between participants with brain aging patterns 1 and 2.

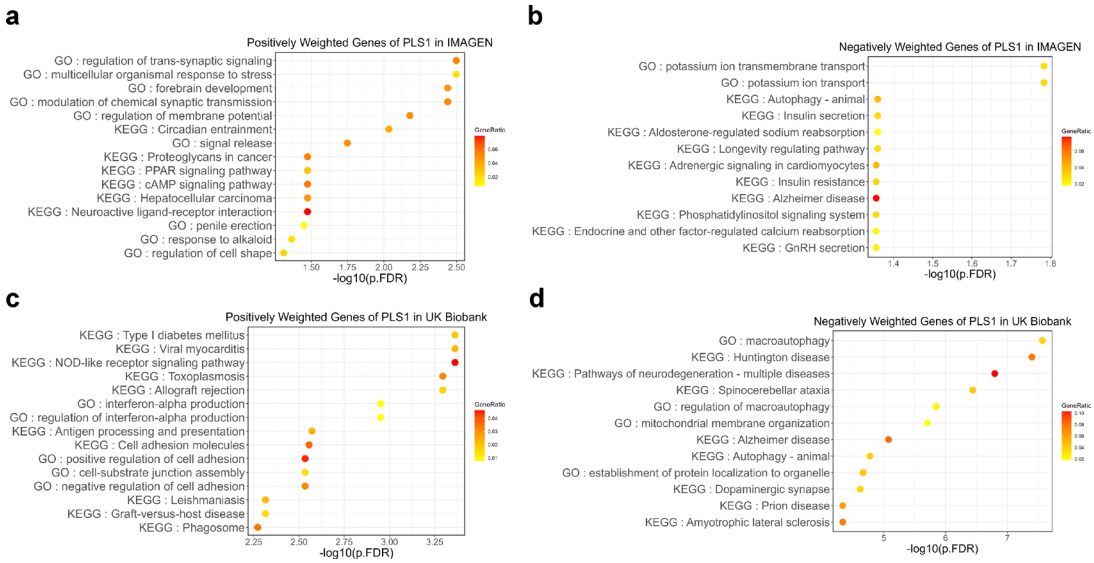

Appendix 1—figure 5. Gene set enrichment of Kyoto Encyclopedia of Genes and Genomes (KEGG) pathways and gene ontology (GO) of biological processes.

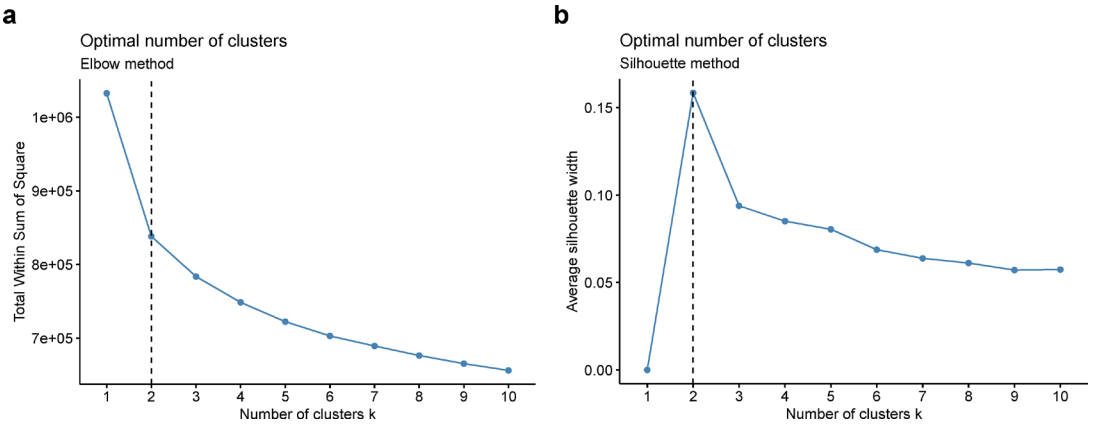

Appendix 1—figure 6. Optimal number of clusters was chosen using elbow method (**a**) and silhouette method (**b**).

Appendix 1—table 1. ICD-10 primary and secondary diagnostic codes for exclusion criteria.

Condition	Code
Malignant neoplasm	C70, C71
Dementia	F00, F01, F02, F03, F04
Mental and behavioural disorders due to psychoactive substance use	F10-F19
Schizophrenia, schizotypal and delusional disorders	F20-F29
Mood [affective] disorders	F30-F39
Mental retardation	F70-F79
Disorders of psychological development	F80-F89
Hyperkinetic disorders	F90
Inflammatory diseases of the central nervous system	G00-G09
Systemic atrophies primarily affecting the central nervous system	G10, G11, G122, G13
Extrapyramidal and movement disorders	G20, G21, G22, G23
Other degenerative diseases of the nervous system	G30-G32
Demyelinating diseases of the central nervous system	G35-G37
Episodic and paroxysmal disorders	G40, G41, G45, G46
Infantile cerebral palsy	G80
Cerebrovascular diseases	I60-I69
Down's syndrome	Q90
Intracranial injury	S06

Appendix 1—table 2. Self-reported illness codes for exclusion criteria.

Field ID	Condition	Code
	Brain cancer/primary malignant brain tumour	1032
20001	Meningeal cancer/malignant meningioma	1031

Appendix 1—table 2 Continued on next page

Appendix 1—table 2 Continued

Field ID	Condition	Code
	Benign neuroma	1683
	Brain abscess/intracranial abscess	1245
	Brain haemorrhage	1491
	Cerebral aneurysm	1425
	Cerebral palsy	1433
	Chronic/degenerative neurological problem	1258
	dementia/alzheimers/cognitive impairment	1263
	Encephalitis	1246
	Epilepsy	1264
	Fracture skull/head	1626
	Head injury	1266
	Ischaemic stroke	1583
	Meningioma/benign meningeal tumour	1659
	Meningitis	1247
	Motor Neurone Disease	1259
	Multiple Sclerosis	1261
	Nervous system infection	1244
	Neurological injury/trauma	1240
	Other demyelinating disease (not Multiple Sclerosis)	1397
	Other neurological problem	1434
	Parkinson's Disease	1262
	Spina Bifida	1524
	Stroke	1081
	Subarachnoid haemorrhage	1086
	Subdural haemorrhage/haematoma	1083
20002	Transient ischaemic attack	1082

Appendix 1—table 3. Cortical and subcortical brain regions.

Desikan–Killiany Atlas
bankssts
caudal anterior cingulate
caudal middle frontal
cuneus
entorhinal
fusiform
inferior parietal
inferior temporal
isthmus cingulate
lateral occipital
lateral orbitofrontal
lingual
medial orbitofrontal
middle temporal
parahippocampal
paracentral
pars opercularis
pars orbitalis
pars triangularis
pericalcarine
postcentral
posterior cingulate
precentral
precuneus
rostral anterior cingulate
rostral middle frontal
superior frontal
superior parietal
superior temporal
supramarginal
frontal pole
transverse temporal
insula
ASEG Atlas
thalamus proper
caudate
putamen
pallidum
hippocampus
amygdala
accumbens area

Appendix 1—table 4. Loadings matrix for the first 15 principal components.

	PC1	PC2	PC3	PC4	PC5	PC6	PC7	PC8	PC9	PC10	PC11	PC12	PC13	PC14	PC15
Cortical															
bankssts	0.12	–0.25	0.01	0.30	–0.13	0.01	0.09	0.34	0.04	0.05	–0.10	0.16	–0.09	–0.20	0.02
caudal.anterior.cingulate	0.12	–0.06	–0.02	0.13	0.39	0.28	0.13	–0.09	–0.37	0.24	0.05	0.03	–0.04	–0.13	0.07
caudal.middle.frontal	0.15	0.01	–0.10	–0.11	0.34	–0.21	0.10	0.06	0.03	–0.28	–0.23	–0.20	0.24	0.00	0.25
cuneus	0.13	0.47	–0.01	0.06	–0.01	0.00	0.07	0.12	0.01	0.07	0.12	–0.05	–0.09	0.08	–0.07
entorhinal	0.09	0.07	0.13	0.08	0.10	0.17	–0.53	–0.18	0.06	0.04	–0.19	–0.10	0.13	0.01	–0.04
fusiform	0.18	–0.03	0.01	0.13	–0.02	0.02	–0.20	–0.02	0.15	0.30	–0.01	–0.28	–0.23	0.08	0.21
inferior.parietal	0.15	–0.18	0.01	0.39	–0.09	0.01	0.14	–0.04	0.16	0.05	–0.20	–0.02	–0.15	–0.02	0.02
inferior.temporal	0.16	–0.13	0.01	0.26	–0.01	0.15	–0.04	–0.10	0.14	–0.08	–0.08	–0.25	0.20	0.29	–0.01
isthmus.cingulate	0.15	0.23	0.02	0.11	–0.14	–0.03	0.08	–0.03	–0.23	–0.07	–0.22	0.16	0.43	0.04	0.11
lateral.occipital	0.16	0.30	0.00	0.12	–0.02	0.02	0.05	0.10	0.16	0.18	0.06	–0.23	–0.23	0.12	0.17
lateral.orbitofrontal	0.22	–0.04	–0.08	–0.17	–0.05	0.15	–0.02	–0.15	0.09	–0.02	–0.01	0.40	–0.01	0.22	0.17
lingual	0.12	0.43	0.03	0.14	–0.01	–0.02	0.07	0.11	–0.01	–0.03	–0.10	0.16	0.02	–0.09	–0.08

Appendix 1—table 4 Continued on next page

Appendix 1—table 4 Continued

	PC1	PC2	PC3	PC4	PC5	PC6	PC7	PC8	PC9	PC10	PC11	PC12	PC13	PC14	PC15
medial.orbitofrontal	0.21	–0.06	–0.06	–0.06	–0.05	0.10	–0.01	–0.13	0.18	–0.06	0.13	0.17	0.05	0.01	–0.25
middle.temporal	0.17	–0.17	–0.01	0.27	–0.14	0.10	0.21	0.25	0.09	–0.15	–0.09	0.04	0.07	0.05	–0.11
parahippocampal	0.12	0.09	0.13	0.05	0.06	0.14	–0.46	0.02	–0.02	0.09	–0.22	0.09	0.03	–0.32	0.02
paracentral	0.19	–0.05	–0.10	–0.07	0.18	–0.23	–0.11	–0.06	0.01	0.03	–0.02	0.06	–0.35	–0.01	–0.35
pars.opercularis	0.16	–0.02	–0.06	–0.23	–0.19	0.10	0.14	0.01	–0.16	–0.13	–0.43	–0.29	–0.16	–0.06	0.00
pars.orbitalis	0.18	0.02	–0.05	–0.17	–0.11	0.24	0.03	–0.17	0.23	0.08	0.01	0.41	–0.14	0.05	0.24
pars.triangularis	0.16	0.02	–0.03	–0.35	–0.26	0.23	0.13	–0.05	–0.06	–0.06	–0.25	–0.17	–0.21	–0.08	–0.05
pericalcarine	0.10	0.47	–0.01	0.08	–0.01	0.01	0.09	0.13	–0.02	–0.01	0.02	0.08	–0.03	0.03	–0.17
postcentral	0.20	–0.04	–0.11	0.06	0.16	–0.29	–0.09	0.12	0.08	0.03	–0.09	0.10	0.04	0.01	0.04
posterior.cingulate	0.18	–0.08	–0.04	0.02	0.24	0.09	0.08	–0.02	–0.30	0.01	–0.07	0.10	–0.05	–0.12	–0.31
precentral	0.21	–0.01	–0.10	–0.08	0.28	–0.29	–0.09	0.08	0.15	–0.05	–0.15	0.13	–0.06	0.05	0.12
precuneus	0.20	0.02	–0.02	0.13	–0.24	–0.26	0.01	–0.35	–0.20	–0.04	0.06	–0.04	0.00	0.03	0.07
rostral.anterior.cingulate	0.15	–0.07	–0.07	0.05	0.31	0.21	0.15	–0.05	–0.30	0.13	0.11	–0.06	0.00	0.18	0.15
rostral.middle.frontal	0.20	0.02	–0.05	–0.05	0.10	0.14	0.22	–0.11	0.17	–0.11	0.24	–0.14	0.19	–0.22	0.14
superior.frontal	0.22	–0.03	–0.09	–0.21	0.14	–0.13	–0.01	0.06	0.20	–0.18	0.06	–0.11	0.02	0.00	–0.16
superior.parietal	0.17	0.02	–0.05	0.14	–0.18	–0.29	0.01	–0.45	–0.16	0.00	0.14	–0.08	–0.08	–0.06	0.04
superior.temporal	0.21	–0.13	–0.02	–0.06	–0.10	0.01	–0.07	0.40	–0.07	0.13	0.24	–0.05	0.02	–0.06	0.08
supramarginal	0.17	–0.15	–0.08	0.06	–0.24	–0.23	–0.13	0.03	–0.21	0.04	0.11	0.10	0.14	–0.08	–0.06
frontal.pole	0.16	0.03	–0.10	0.01	0.00	0.16	0.03	–0.13	0.28	0.05	0.28	–0.16	0.26	–0.38	–0.22
transverse.temporal	0.15	–0.01	–0.10	–0.27	–0.17	–0.10	–0.16	0.25	–0.22	0.19	0.24	–0.10	0.09	0.04	0.16
insula	0.19	–0.08	0.01	–0.22	–0.12	0.10	–0.07	0.11	–0.06	0.15	–0.08	0.00	0.19	0.16	–0.23
Subcortical															
thalamus.proper	0.09	–0.02	0.31	–0.08	0.03	–0.08	0.08	0.00	0.02	–0.21	0.11	0.10	–0.19	–0.37	0.33
caudate	0.06	–0.03	0.32	–0.12	0.02	–0.10	0.15	–0.02	0.11	0.31	–0.11	0.09	0.27	0.14	0.12
putamen	0.08	–0.03	0.42	–0.12	0.03	–0.13	0.13	–0.03	0.05	0.22	–0.05	–0.14	0.07	–0.02	–0.17
pallidum	0.03	–0.03	0.42	–0.07	0.00	–0.13	0.16	–0.06	0.04	0.20	–0.07	0.00	0.04	–0.20	–0.06
hippocampus	0.12	0.01	0.33	0.04	–0.02	0.11	–0.20	0.08	–0.16	–0.39	0.09	0.03	–0.11	–0.03	0.05
amygdala	0.13	–0.03	0.31	0.05	–0.01	0.12	–0.13	0.09	–0.07	–0.35	0.25	–0.09	–0.02	0.24	–0.01
accumbens.area	0.11	–0.05	0.31	–0.02	0.12	–0.07	0.11	–0.04	0.00	–0.03	0.10	0.09	–0.14	0.34	–0.18

Appendix 1—table 5. Baseline and demographic characteristics for participants in the total population and stratified by brain aging patterns.

	Total (n=37,013)	Pattern 1 (n=18,929)	Pattern 2 (n=18,084)
Age (years), mean (SD)	63.9 (7.63)	63.9 (7.64)	63.8 (7.63)
Female, n (%)	19,958 (53.9)	10,117 (53.4)	9,841 (54.4)
Ethnicity, n (%)			
White	34,219 (92.5)	17,509 (92.5)	16,710 (92.4)
Mixed	1,137 (3.1)	573 (3.0)	564 (3.1)
Asian or Asian British	1,210 (3.3)	612 (3.2)	598 (3.3)
Other	447 (1.2)	235 (1.2)	212 (1.2)

Appendix 1—table 5 Continued on next page

Appendix 1—table 5 Continued

	Total (n=37,013)	Pattern 1 (n=18,929)	Pattern 2 (n=18,084)
Smoking status, n (%)*			
Never smoker	23,633 (64.4)	12,269 (65.4)	11,364 (63.4)
Previous smoker	12,213 (33.3)	6,085 (32.4)	6,128 (34.2)
Current smoker	833 (2.3)	414 (2.2)	419 (2.3)
TDI, mean (SD)†	–1.94 (2.69)	–1.97 (2.66)	–1.90 (2.71)
BMI (kg/m^2), mean (SD)‡	26.4 (4.32)	26.3 (4.17)	26.5 (4.46)
Years of Schooling, mean (SD)§	16.8 (4.32)	16.9 (4.29)	16.8 (4,35)

TDI = Townsend Deprivation Index, BMI = Body Mass Index.
*Missing 334
†Missing 36
‡Missing 1937
§Missing 337

Appendix 1—table 6. Associations between results of biological aging biomarkers and subgroups stratified by whole-brain TGMV trajectories.
Cohen's d measures the standardized difference of means between brain aging pattern 2 and brain aging pattern 1.

Biological aging biomarkers	Brain aging pattern 1		Brain aging pattern 2			
	N	Mean(SD)	N	Mean(SD)		
LTL	17,691	0.083 (0.98)	16,876	0.055 (0.97)		
PhenoAge	15,228	41.35 (8.17)	14,323	41.58 (8.32)		
Biological aging biomarkers	Unadjusted			Adjusted		
	Cohen's d (95% CI)	p	P.Bonferroni	Cohen's d (95% CI)	p	P.Bonferroni
LTL	–0.028 (-0.049,–0.007)	0.009	0	–0.030 (-0.051,–0.009)	0.006	0.011
PhenoAge	0.027 (0.004, 0.050)	0.019	0	0.092 (0.070, 0.116)	3.05E-15	6.11E-15

Appendix 1—table 7. Associations between results of cognitive function tests and subgroups stratified by whole-brain TGMV trajectories.
Cohen's d measures the standardized difference of means between brain aging pattern 2 and brain aging pattern 1.

Cognitive functions	Brain aging pattern 1		Brain aging pattern 2	
	N	Mean(SD)	N	Mean(SD)
Reaction time	17,749	–594.70 (108.15)	16,831	–594.68 (110.50)
Numeric memory	13,350	6.82 (1.26)	12,346	6.72 (1.27)
Fluid intelligence	17,580	6.73 (2.06)	16,612	6.53 (2.04)
Trail making A	13,052	–224.50 (84.82)	12,036	–227.56 (84.85)
Trail making B	12,743	–563.06 (246.74)	11,753	–576.55 (260.75)
Matrix pattern completion	13,064	8.07 (2.11)	12,064	7.91 (2.14)
Symbol digit substitution	13,077	19.08 (5.15)	12,056	18.87 (5.35)
Tower rearranging	12,952	9.96 (3.20)	11,958	9.83 (3.23)

Appendix 1—table 7 Continued on next page

Appendix 1—table 7 Continued

	Brain aging pattern 1			Brain aging pattern 2		
Cognitive functions	**N**	**Mean(SD)**		**N**	**Mean(SD)**	
Paired associate learning	13,184	7.01 (2.59)		12,198	6.88 (2.65)	
Prospective memory	17,831	N/A		16,949	N/A	
Pairs matching	17,840	–3.58 (2.90)		16,956	–3.67 (2.94)	
	Unadjusted			Adjusted		
Cognitive functions	Cohen's d (95% CI)	P	P.FDR	Cohen's d (95% CI)	P	P.FDR
Reaction time	0.000 (-0.021, 0.021)	0.99	0.99	0.006 (-0.016, 0.028)	0.61	0.61
Numeric memory	–0.082 (-0.106,–0.057)	5.97E-11	3.28E-10	–0.080 (-0.106,–0.055)	8.99E-10	4.95E-09
Fluid intelligence	–0.102 (-0.123,–0.080)	5.94E-21	6.54E-20	–0.99 (-0.121,–0.077)	3.30E-18	3.63E-17
Trail making A	–0.036 (-0.061,–0.011)	0.004	0.006	–0.050 (-0.074,–0.024)	1.46E-04	2.29E-04
Trail making B	–0.053 (-0.078,–0.028)	3.16E-05	8.68E-05	–0.067 (-0.093,–0.041)	6.16E-07	1.69E-06
Matrix pattern completion	–0.076 (-0.101,–0.051)	1.84E-09	6.74E-09	–0.078 (-0.104,–0.052)	3.67E-09	1.35E-08
Symbol digit substitution	–0.040 (-0.065,–0.015)	0.002	0.002	–0.053 (-0.079,–0.027)	6.15E-05	1.13E-04
Tower rearranging	–0.041 (-0.066,–0.016)	0.001	0.002	–0.049 (-0.075,–0.023)	2.18E-04	3.00E-04
Paired associate learning	–0.051 (-0.076,–0.027)	4.64E-05	1.02E-04	–0.054 (-0.079,–0.028)	4.89E-05	1.08E-04
Prospective memory	OR: 0.943 (0.891, 0.999)	0.047	0.052	OR: 0.940 (0.883, 1.000)	0.052	0.057
Pairs matching	–0.029 (-0.050,–0.008)	0.006	0.008	–0.033 (-0.055,–0.011)	0.003	0.004

Appendix 1—table 8. Genome-wide association study details.
Loci associated with risk were thresholded at $p<5\times10^{-8}$, then distance-based clumping was used to define independently significant loci.

Study	Number cases	Number controls	Number of genome-wide independently significant loci	Download link
Attention deficit hyperactivity disorder ***Demontis et al., 2019***	20,183	35,191	12	https://figshare.com/ndownloader/files/28169253
Autism spectrum disorder ***Grove et al., 2019***	18,381	27,969	5	https://figshare.com/ndownloader/files/28169292
Alzheimer's disease ***Jansen et al., 2019***	71,880	383,378	25	https://ctg.cncr.nl/software/summary_statistics
Parkinson's disease ***Nalls et al., 2019***	37,688, and 18,618 (proxy-cases)	1,417,791	90	https://drive.google.com/file/d/1FZ9UL99LAqyWnyNBxxlx6qOUlfAnublN/view?usp=sharing

Appendix 1—table 8 Continued on next page

Appendix 1—table 8 Continued

Study	Number cases	Number controls	Number of genome-wide independently significant loci	Download link
Bipolar disorder ***Mullins et al., 2021***	41,917	371,549	64	https://figshare.com/ndownloader/files/40036705
Major depressive disorder ***Wray et al., 2018***	135,458	344,901	44	https://figshare.com/ndownloader/files/39504667
Schizophrenia ***Trubetskoy et al., 2022***	76,755	243,649	287	https://figshare.com/ndownloader/files/34517828
Delayed Brain Development ***Shi et al., 2023***	7662 (proxy phenotype, continuous)		1	https://delayedneurodevelopment.page.link/amTC

Appendix 1—table 9. Polygenic Risk Scores comparisons between two subgroups.
Data supporting these scores were obtained either entirely from external GWAS data (the Standard PRS set). The bold P values reflect significance after FDR correction.

Trait	n1	n2	statistic	p	p.adjust
AAM	18,429	17,586	–2.218	0.027	0.080
AMD	18,429	17,586	1.753	0.080	0.169
AD	18,429	17,586	0.735	0.462	0.616
AST	18,429	17,586	–0.861	0.389	0.543
AF	18,429	17,586	–0.100	0.920	0.945
BD	18,429	17,586	3.557	3.75E-04	0.002
BMI	18,429	17,586	–3.309	0.001	0.005
CRC	18,429	17,586	–0.544	0.586	0.703
BC	18,429	17,586	–3.140	0.002	0.008
CVD	18,429	17,586	–2.104	0.035	0.091
CED	18,429	17,586	1.046	0.296	0.484
CAD	18,429	17,586	–1.588	0.112	0.202
CD	18,429	17,586	–0.094	0.925	0.945
EOC	18,429	17,586	–2.183	0.029	0.080
EBMDT	18,429	17,586	–11.343	<1.00E-20	<1.00E-20
HBA1C_DF	18,429	17,586	–2.948	0.003	0.013
HEIGHT	18,429	17,586	6.658	2.81E-11	3.37E-10
HDL	18,429	17,586	0.884	0.377	0.543
HT	18,429	17,586	–3.539	4.02E-04	0.002
IOP	18,429	17,586	–1.605	0.109	0.202
ISS	18,429	17,586	–2.383	0.017	0.056
LDL_SF	18,429	17,586	–0.686	0.492	0.627
MEL	18,429	17,586	2.025	0.043	0.103
MS	18,429	17,586	–0.069	0.945	0.945
OP	18,429	17,586	12.029	<1.00E-20	<1.00E-20

Appendix 1—table 9 Continued on next page

Appendix 1—table 9 Continued

Trait	n1	n2	statistic	p	p.adjust
PD	18,429	17,586	1.456	0.145	0.249
POAG	18,429	17,586	–0.856	0.392	0.543
PC	18,429	17,586	–0.240	0.810	0.941
PSO	18,429	17,586	–1.781	0.075	0.169
RA	18,429	17,586	–2.437	0.015	0.053
SCZ	18,429	17,586	0.158	0.874	0.945
SLE	18,429	17,586	1.695	0.090	0.180
T1D	18,429	17,586	0.666	0.505	0.627
T2D	18,429	17,586	–5.523	3.35E-08	3.02E-07
UC	18,429	17,586	0.883	0.377	0.543
VTE	18,429	17,586	–0.170	0.865	0.945

Appendix 1—table 10. Polygenic Risk Scores comparisons between two subgroups.
Data supporting these scores were obtained external and internal UK Biobank data (the Enhanced PRS set). The bold p values reflect significance after FDR correction.

Trait	n1	n2	statistic	p	p.adjust
AAM	3,407	3,409	–1.708	0.088	0.344
AMD	3,407	3,409	0.547	0.584	0.931
AD	3,407	3,409	0.756	0.450	0.820
APOEA	3,407	3,409	0.023	0.982	0.993
APOEB	3,407	3,409	0.119	0.905	0.968
AST	3,407	3,409	0.112	0.911	0.968
AF	3,407	3,409	1.306	0.192	0.600
BD	3,407	3,409	0.561	0.575	0.931
BMI	3,407	3,409	–0.976	0.329	0.730
CRC	3,407	3,409	0.984	0.325	0.730
BC	3,407	3,409	–0.995	0.320	0.730
CAL	3,407	3,409	–1.786	0.074	0.326
CVD	3,407	3,409	–0.009	0.993	0.993
CED	3,407	3,409	1.280	0.200	0.600
CAD	3,407	3,409	0.231	0.818	0.961
DOA	3,407	3,409	–0.326	0.745	0.961
EOC	3,407	3,409	–2.167	0.030	0.155
EBMDT	3,407	3,409	–6.111	1.04E-09	2.65E-08
EGCR	3,407	3,409	0.413	0.680	0.961
EGCY	3,407	3,409	–0.210	0.834	0.961
HBA1C_DF	3,407	3,409	0.130	0.896	0.968
HEIGHT	3,407	3,409	4.351	1.38E-05	2.35E-04
HDL	3,407	3,409	0.294	0.769	0.961
HT	3,407	3,409	–0.884	0.377	0.743

Appendix 1—table 10 Continued on next page

Appendix 1—table 10 Continued

Trait	n1	n2	statistic	p	p.adjust
IOP	3,407	3,409	–2.366	0.018	0.151
ISS	3,407	3,409	0.066	0.947	0.986
LDL_SF	3,407	3,409	–0.193	0.847	0.961
MEL	3,407	3,409	2.659	0.008	0.080
MS	3,407	3,409	–2.293	0.022	0.151
OTFA	3,407	3,409	0.318	0.750	0.961
OSFA	3,407	3,409	0.770	0.441	0.820
OP	3,407	3,409	6.484	9.54E-11	4.87E-09
PD	3,407	3,409	1.041	0.298	0.730
PDCL	3,407	3,409	0.663	0.507	0.862
PHG	3,407	3,409	0.392	0.695	0.961
PFA	3,407	3,409	0.495	0.621	0.932
POAG	3,407	3,409	–1.083	0.279	0.730
PC	3,407	3,409	0.675	0.500	0.862
PSO	3,407	3,409	–2.234	0.026	0.151
RMNC	3,407	3,409	0.501	0.617	0.932
RHR	3,407	3,409	–2.865	0.004	0.053
RA	3,407	3,409	0.297	0.766	0.961
SCZ	3,407	3,409	–0.880	0.379	0.743
SGM	3,407	3,409	–0.224	0.823	0.961
SLE	3,407	3,409	1.458	0.145	0.493
TCH	3,407	3,409	0.191	0.848	0.961
TFA	3,407	3,409	0.892	0.372	0.743
TTG	3,407	3,409	1.212	0.226	0.640
T1D	3,407	3,409	1.771	0.077	0.326
T2D	3,407	3,409	–2.218	0.027	0.151
VTE	3,407	3,409	–1.613	0.107	0.390

Appendix 1—table 11. Most significant single-variant associations ($p < 510^{-8}$) detected in the GWAS analyses.

Six independent SNPs at genome-wide significance level were identified by linkage disequilibrium (LD) clumping (r2 < 0.1 within a 250 kb window). The location (chromosome [chr] and base position [bp]), alleles (A1 = effect allele and A2 = other allele), effect (β) and its standard error (β SE) with respect to A1, and association p-values from regression model of the variants are given, along with functional consequences of SNPs on gene by performing ANNOVAR.

SNP	A1	A2	p-value	β	β SE	Location (chr:bp)	Gene symbol	Position relative to gene
rs10835187	C	T	1.70e-14	–0.02558	0.003333	11:27505677	LGR4, LIN7C	intergenic
rs7776725	C	T	4.47e-13	–0.02640	0.003644	7:121033121	FAM3C	intronic
rs779233904	AAC	A	1.57e-09	0.02083	0.003449	6:151910404	CCDC170	intronic
rs2504071	T	C	3.34e-09	0.01959	0.003311	6:152084862	ESR1	intronic
17:43553496:A:AAT	A	AAT	6.65e-09	–0.02472	0.004261	17:43553496	PLEKHM1	intronic

Appendix 1—table 11 Continued on next page

Appendix 1—table 11 Continued

SNP	A1	A2	p-value	β	β SE	Location (chr:bp)	Gene symbol	Position relative to gene
10:104227791:G:GA	GA	G	1.48e-08	–0.01889	0.003334	10:104227791	TMEM180	intronic

Appendix 1—table 12. Association between gene expression profiles of mapped genes and estimated APC during brain development.
The bold p values reflect significance after the spatial permutation test.

Gene Symbol	Spearman's ρ	p value	P.permutation
ACTR1A	0.096	0.440	0.328
ARHGAP27	0.051	0.684	0.445
ARL17B	0.047	0.705	0.452
BDNF-AS	0.256	0.038	0.038
CCDC170	0.268	0.030	0.069
ESR1	0.021	0.870	0.483
FAM3C	–0.096	0.444	0.356
KANSL1	–0.262	0.034	0.073
KANSL1-AS1	0.067	0.594	0.313
LGR4	0.558	1.78E-06	2.50E-04
LIN7C	0.036	0.775	0.464
LRRC37A4P	–0.272	0.027	0.148
MAPT	0.024	0.846	0.405
PLEKHM1	–0.276	0.025	0.109
SPPL2C	0.116	0.351	0.189
STH	–0.147	0.238	0.277
SUFU	0.407	0.001	0.028

Appendix 1—table 13. Association between gene expression profiles of mapped genes and estimated APC during brain aging.
The bold p values reflect significance after the spatial permutation test.

Gene Symbol	Spearman's ρ	Pvalue	P.permutation
ACTR1A	–0.235	0.058	0.052
ARHGAP27	0.486	4.48E-05	5.50E-04
ARL17B	0.090	0.473	0.240
BDNF-AS	0.490	3.68E-05	1.50E-04
CCDC170	0.206	0.098	0.075
ESR1	0.532	6.02E-06	1.50E-04
FAM3C	–0.366	0.003	0.005
KANSL1	0.213	0.086	0.078
KANSL1-AS1	–0.262	0.034	0.059
LGR4	0.070	0.576	0.348
LIN7C	0.177	0.154	0.120
LRRC37A4P	0.143	0.250	0.165

Appendix 1—table 13 Continued on next page

Appendix 1—table 13 Continued

Gene Symbol	Spearman's ρ	Pvalue	P.permutation
MAPT	–0.287	0.020	0.022
PLEKHM1	0.202	0.104	0.080
SPPL2C	0.211	0.089	0.059
STH	–0.001	0.997	0.490
SUFU	–0.036	0.773	0.373

Appendix 1—table 14. Model evaluation results using relative measures: AIC, BIC, likelihood ratio test and intra-class correlation (ICC).

model	AIC	BIC	lrtest	ICC_adjusted	ICC_unadjusted
lmer_intr_thalamus.proper	79444.24	79591.29	6.45E-15	0.8875	0.3958
lmer_slope_thalamus.proper	79382.89	79547.24	6.45E-15	0.8889	0.3986
lmer_intr_caudate	95845.48	95992.54	2.68E-71	0.9543	0.6824
lmer_slope_caudate	95524.49	95688.84	2.68E-71	0.9564	0.6817
lmer_intr_putamen	92106.06	92253.12	2.40E-42	0.9398	0.5946
lmer_slope_putamen	91918.4	92082.75	2.40E-42	0.9424	0.5933
lmer_intr_pallidum	90500.3	90647.36	4.21E-42	0.8859	0.5116
lmer_slope_pallidum	90313.76	90478.12	4.21E-42	0.8862	0.5093
lmer_intr_hippocampus	89833.92	89980.97	1.37E-08	0.9309	0.5505
lmer_slope_hippocampus	89801.71	89966.06	1.37E-08	0.9329	0.5505
lmer_intr_amygdala	89976.98	90124.03	4.01E-06	0.8697	0.4898
lmer_slope_amygdala	89956.13	90120.48	4.01E-06	0.8713	0.4897
lmer_intr_accumbens.area	96936.19	97083.24	1.69E-14	0.8228	0.5295
lmer_slope_accumbens.area	96876.77	97041.12	1.69E-14	0.8233	0.5310
lmer_intr_bankssts	97981.96	98129.01	0.001818	0.9339	0.6798
lmer_slope_bankssts	97973.34	98137.69	0.001818	0.9354	0.6814
lmer_intr_caudal.anterior.cingulate	109133.2	109280.3	0.131507	0.8638	0.7653
lmer_slope_caudal.anterior.cingulate	109133.2	109297.5	0.131507	0.8644	0.7659
lmer_intr_caudal.middle.frontal	93118.13	93265.19	8.31E-06	0.9227	0.5929
lmer_slope_caudal.middle.frontal	93098.74	93263.09	8.31E-06	0.9246	0.5949
lmer_intr_cuneus	101801.4	101948.5	0.014429	0.9242	0.7256
lmer_slope_cuneus	101796.9	101961.3	0.014429	0.9245	0.7262
lmer_intr_entorhinal	109404.9	109551.9	1.63E-14	0.8013	0.6908
lmer_slope_entorhinal	109345.4	109509.7	1.63E-14	0.8037	0.6928
lmer_intr_fusiform	87545.88	87692.93	9.17E-05	0.9139	0.5062
lmer_slope_fusiform	87531.28	87695.63	9.17E-05	0.9163	0.5074
lmer_intr_inferior.parietal	89044.43	89191.48	5.89E-14	0.9374	0.5564
lmer_slope_inferior.parietal	88987.51	89151.86	5.89E-14	0.9419	0.5603
lmer_intr_inferior.temporal	84066.47	84213.52	5.73E-07	0.9384	0.4956
lmer_slope_inferior.temporal	84041.73	84206.08	5.73E-07	0.9405	0.4977
lmer_intr_isthmus.cingulate	92442.12	92589.17	0.127191	0.9275	0.5862

Appendix 1—table 14 Continued on next page

Appendix 1—table 14 Continued

model	AIC	BIC	lrtest	ICC_adjusted	ICC_unadjusted
lmer_slope_isthmus.cingulate	92442	92606.35	0.127191	0.9284	0.5869
lmer_intr_lateral.occipital	89550.4	89697.45	0.003943	0.9121	0.5273
lmer_slope_lateral.occipital	89543.33	89707.68	0.003943	0.9129	0.5282
lmer_intr_lateral.orbitofrontal	86224.13	86371.18	1.29E-08	0.8466	0.4323
lmer_slope_lateral.orbitofrontal	86191.79	86356.14	1.29E-08	0.8497	0.4345
lmer_intr_lingual	102605.2	102752.2	0.041242	0.9181	0.7268
lmer_slope_lingual	102602.8	102767.2	0.041242	0.9181	0.7272
lmer_intr_medial.orbitofrontal	89954.36	90101.41	2.25E-06	0.7832	0.4219
lmer_slope_medial.orbitofrontal	89932.35	90096.7	2.25E-06	0.7872	0.4241
lmer_intr_middle.temporal	83331.01	83478.06	0.0019	0.9177	0.4615
lmer_slope_middle.temporal	83322.48	83486.83	0.0019	0.9195	0.4629
lmer_intr_parahippocampal	108997.1	109144.2	4.99E-05	0.8686	0.7639
lmer_slope_parahippocampal	108981.3	109145.6	4.99E-05	0.8690	0.7639
lmer_intr_paracentral	98058.63	98205.68	0.015686	0.8695	0.5958
lmer_slope_paracentral	98054.32	98218.67	0.015686	0.8705	0.5960
lmer_intr_pars.opercularis	96829.05	96976.1	1.20E-12	0.9354	0.6658
lmer_slope_pars.opercularis	96778.15	96942.5	1.20E-12	0.9396	0.6698
lmer_intr_pars.orbitalis	96989.61	97136.67	1.39E-05	0.8785	0.5892
lmer_slope_pars.orbitalis	96971.25	97135.6	1.39E-05	0.8805	0.5912
lmer_intr_pars.triangularis	96637.58	96784.63	4.55E-18	0.9402	0.6710
lmer_slope_pars.triangularis	96561.72	96726.07	4.55E-18	0.9439	0.6748
lmer_intr_pericalcarine	105115.9	105263	0.022841	0.9429	0.8190
lmer_slope_pericalcarine	105112.4	105276.7	0.022841	0.9441	0.8200
lmer_intr_postcentral	91605.6	91752.65	0.000549	0.8764	0.5189
lmer_slope_postcentral	91594.59	91758.94	0.000549	0.8789	0.5203
lmer_intr_posterior.cingulate	96853.73	97000.78	2.21E-19	0.8913	0.6014
lmer_slope_posterior.cingulate	96771.82	96936.17	2.21E-19	0.8949	0.6022
lmer_intr_precentral	91186.59	91333.64	2.61E-12	0.8478	0.4864
lmer_slope_precentral	91137.25	91301.6	2.61E-12	0.8504	0.4864
lmer_intr_precuneus	84734.58	84881.63	1.23E-08	0.9088	0.4708
lmer_slope_precuneus	84702.16	84866.51	1.23E-08	0.9126	0.4730
lmer_intr_rostral.anterior.cingulate	95688.68	95835.73	2.64E-12	0.9093	0.6097
lmer_slope_rostral.anterior.cingulate	95639.36	95803.72	2.64E-12	0.9122	0.6129
lmer_intr_rostral.middle.frontal	80873.84	81020.89	2.57E-17	0.9137	0.4354
lmer_slope_rostral.middle.frontal	80801.44	80965.79	2.57E-17	0.9191	0.4395
lmer_intr_superior.frontal	79730.6	79877.65	1.25E-11	0.8921	0.4038
lmer_slope_superior.frontal	79684.38	79848.73	1.25E-11	0.8972	0.4060
lmer_intr_superior.parietal	92895.95	93043	8.55E-07	0.8899	0.5487

Appendix 1—table 14 Continued on next page

Appendix 1—table 14 Continued

model	AIC	BIC	lrtest	ICC_adjusted	ICC_unadjusted
lmer_slope_superior.parietal	92872.01	93036.36	8.55E-07	0.8934	0.5512
lmer_intr_superior.temporal	86495.24	86642.29	0.003021	0.9148	0.4959
lmer_slope_superior.temporal	86487.64	86651.99	0.003021	0.9168	0.4971
lmer_intr_supramarginal	87390.39	87537.44	3.67E-13	0.9263	0.5221
lmer_slope_supramarginal	87337.12	87501.47	3.67E-13	0.9320	0.5258
lmer_intr_frontal.pole	110426.3	110573.4	1.95E-65	0.6907	0.5868
lmer_slope_frontal.pole	110132.3	110296.7	1.95E-65	0.6957	0.5882
lmer_intr_transverse.temporal	102753.2	102900.2	0.032413	0.9130	0.7247
lmer_slope_transverse.temporal	102750.3	102914.7	0.032413	0.9144	0.7258
lmer_intr_insula	88693.2	88840.26	7.61E-14	0.8263	0.4416
lmer_slope_insula	88636.79	88801.14	7.61E-14	0.8290	0.4420